CONSTRUCTION OF A SHEETED DYKE COMPLEX: EVIDENCE FROM THE NORTHERN MARGIN OF THE TROODOS OPHIOLITE AND ITS SOUTHERN MARGIN ADJACENT TO THE ARAKAPAS FAULT ZONE

Alexander J. Cooke, Lee P. Masson and **Alastair H.F. Robertson** ✉

School of GeoSciences, University of Edinburgh, U.K.
✉ *Corresponding author email: Alastair.Robertson@ed.ac.uk*

Keywords: *Troodos ophiolite, sheeted dykes, transform fault, geochemistry, structure.*

ABSTRACT

The structure of a sheeted dyke complex in relation to intrusion is important for an understanding of sea-floor spreading. Here, we provide data for a previously undescribed ~ E-W cross-strike section along the northern margin of the Troodos Massif. For comparison, we also provide new information for a ~N-S section along the southern margin of the Troodos Massif, adjacent to the Arakapas Fault Zone, an inferred oceanic transform fault.

The N-Troodos margin section is divided into two main segments with opposing dip directions, corresponding to the Solea Graben in the east and the Stravros Graben in the west. High-temperature, hydrothermally altered dykes occur relatively early in a relative intrusive chronology of both grabens, followed by gabbroic bodies and ubiquitous grey sheeted dykes; plagiogranite dykes intruded at relatively later stages. Chemical analyses reveals a trend towards a boninite-type composition, both in the sheeted complex as a whole and in several specific sections for which crosscutting relations were documented in detail. The relatively steeply dipping, late-stage, boninitic-type dykes are interpreted as feeders to the Upper Pillow Lavas.

To the N of the Arakapas Fault Zone, large plagiogranite bodies intruded relatively early and were in turn transected by grey dykes, small gabbroic intrusions and late-stage isolated brown dykes. Chemical analyses show that both early-stage grey dykes and the later-stage brown dykes were fed by chemically similar magma. Highly depleted boninite-type dykes occur close to the Arakapas Fault Zone. The relatively late-stage brown dykes show a swing in orientation towards ~ E-W near the transform zone, reflecting an inferred up to ~ 90° relatively clockwise, vertical-axis rotation. The earlier-stage grey dykes are indicative of lesser amounts of vertical-axis rotation but show complex rotations about low-angle axes. Small-scale faults are mainly of normal and left-lateral strike-slip type. Taking alternatives into account, we infer that the faulting in the dyke section took place near a left-offset spreading axis within an overall right-slipping, transtensional transform fault zone. In addition, depleted mantle harzburgites were exposed and eroded on the seafloor within an inferred southward extension of the transform zone (now within the Late Cretaceous Moni Mélange), proving additional evidence of a transtensional setting near or within the Arakapas transform.

The combined evidence suggests that the Troodos sheeted dyke complex as a whole developed in response to unstable, asymmetrical spreading above a subduction zone in which relatively late-stage amagmatic extension is likely to have played an important role. The spreading crust was bounded to the south (in present coordinates) by a relatively broad transtensional transform fault zone, along which mantle rocks were locally exposed and eroded on the seafloor.

INTRODUCTION

Sheeted dykes in ophiolites play a key role in our understanding of sea floor spreading processes (Gass, 1968; Moores and Vine, 1971; Cann and Gillis, 2004). It is generally assumed that observations in ophiolites, notably the Troodos, may be indicative of processes operating at oceanic spreading axes and vice versa (Robertson and Xenophontos, 1993). However, it is debateable as to what extent ophiolites, such as the Troodos, formed in the same manner as mid-ocean ridges (Robinson et al., 2008), especially since the Troodos is generally accepted to have formed above a subduction zone (Pearce and Robinson, 2010).

At an early stage in the development of plate tectonics theory, sheeted dykes were recognised within the Troodos ophiolite (Fig. 1) and interpreted as the result of sea-floor spreading within the Mesozoic Tethys (Gass, 1968; Moores and Vine, 1971). The surface outcrops of the sheeted dykes were studied, petrographically and geochemically at a relatively early stage in research on the Troodos ophiolite (Desmet et al., 1978; Baragar et al., 1989; Moores and Vine, 1971). Additional subsurface data were obtained from drill hole CY-4 during the Cyprus Crustal Study Project (Baragar et al., 1990). Zones of shearing and faulting were identified in several areas (Baragar et al., 1989; 1990). Detailed structural studies of some parts of the sheeted dyke complex later revealed the importance of extensional faulting in the construction of the Troodos sheeted complex (Dietrich and Spencer, 1993). However, little attempt has previously been made to relate the lithology and geochemistry of intrusion to the outcrop-scale structure in detail (but see Veit, 1996).

The sheeted dykes are generally orientated ~ N-S owing to the well documented 90° anticlockwise palaeo-rotation of the Troodos Massif, based on palaeomagnetic studies (Moores and Vine, 1971; Clube et al., 1985; Morris et al., 1990). In the south, the Troodos Massif is truncated by the prominent east-west trending Arakapas Fault Zone, which is also known as the South Troodos Transform Fault Zone (Fig. 1). The name Arakapas Fault Zone is preferred here so as not to presume any particular setting of formation (i.e. a non-genetic name is preferable). The fault zone is generally accepted to represent an oceanic transform fault zone that was contemporaneous with the formation of the Troodos ophiolite (Moores and Vine, 1971; Simonian and Gass, 1978; Gass et al., 1994; MacLeod and Murton, 1995).

Despite decades of productive research in Cyprus, surprisingly little consensus has yet emerged concerning the processes of sea-floor spreading or transform faulting that gave rise to the Troodos ophiolite. Seafloor spreading is inferred to have taken place, either progressively at a single spreading centre (Kidd and Cann, 1974; Cann and Gillis, 2004; Allerton and Vine, 1987), or episodically, involving step-wise relocation of a spreading centre (Varga and Moores, 1985; 1990; Hurst et al., 1994). For the Arakapas transform, in present coordinates, the slip direction was right-lateral in some interpretations (Clube et al., 1985; Clube and Robertson, 1986; Murton, 1986; Allerton, 1988; Morris et al., 1990; Gass et al., 1994; MacLeod and Murton, 1995;

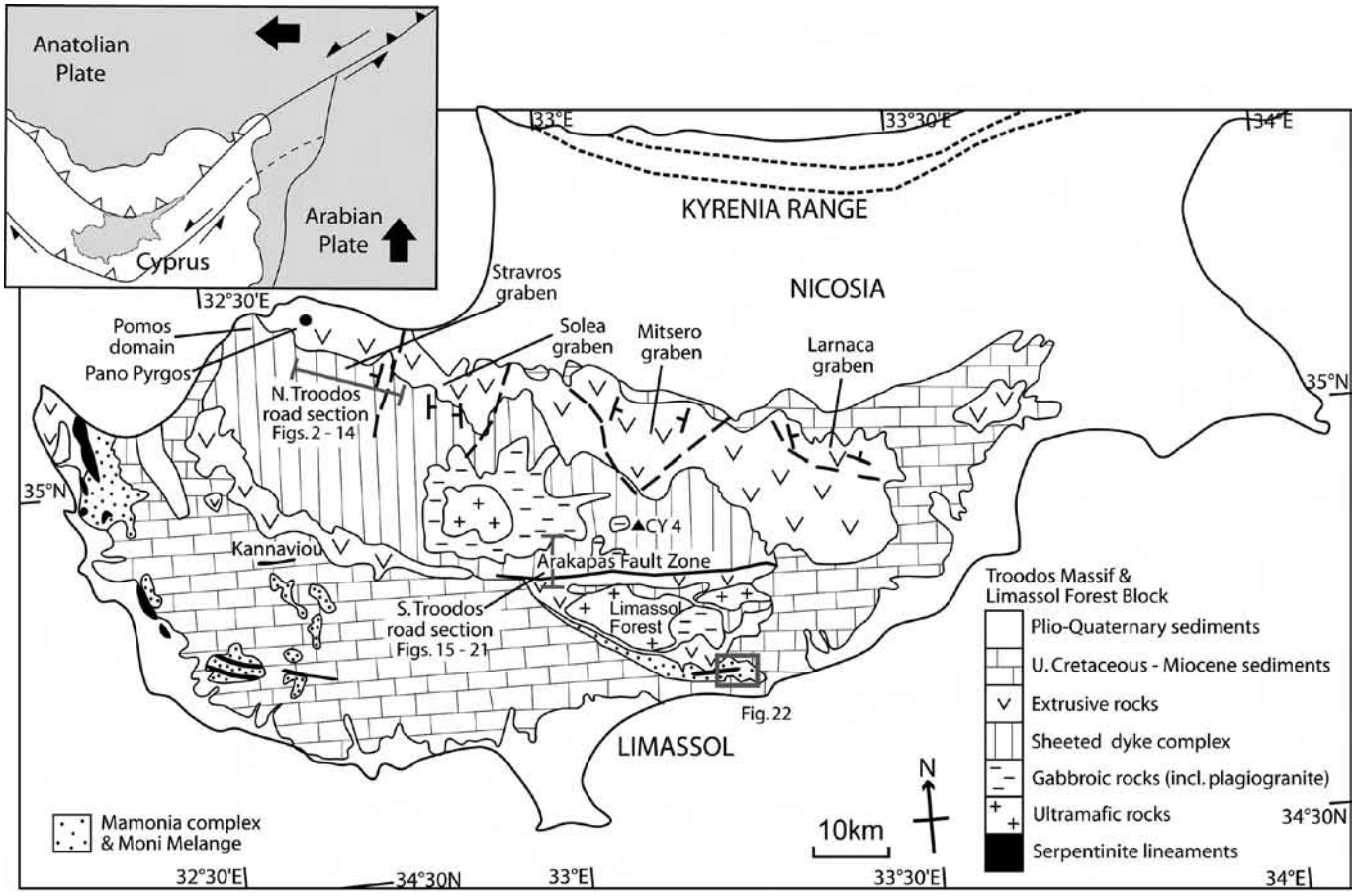

Fig. 1 - Outline tectonic map of the Troodos ophiolite showing the extensional grabens within the spreading fabric and also the Arakapas Fault Zone (~ South Troodos Transform Fault Zone). Note the locations of the study sections along the northern and southern margins of the Troodos Massif, namely the Pyrgos road section and the south-Troodos road section. In addition, a small area of ophiolite-related in the south that is relevant to the interpretation of the Arakapas Fault Zone is marked by the box.

Morris, l996; Abelson et al., 2002; Granot et al., 2006; Borradaile and Gauthier, 2006; Scott et al., 2012), but left-lateral in others (Simonian and Gass, l978; Varga and Moores, l985; Cann et al., 2001; 2004). Detailed analyses of the regional dyke trends has recently been carried out, supplemented by the collection of new data from a wide region of the southern Troodos Massif (Scott et al., 2012). These authors used the combined data to test several alternative mechanisms of spreading and deformation in the vicinity of the Arakapas Fault Zone. However, they note a need for more field data particularly on the relative timing of intrusion and deformation of the sheeted dykes.

The aim of this paper is to present and interpret the results of two field-based pilot studies of the sheeted dyke complex, one in relation to spreading processes in a representative part of the northern outcrop of the Troodos ophiolite (Masson, 2012) and the other in relation to spreading processes near the Arakapas Fault Zone in the south (Cooke, 2013). Two comparative sections were studied, one along the northern margin of the Troodos Massif and one along the southern margin of the Troodos Massif (Fig. 1). The northern Troodos section is an excellent example of a sheeted dyke complex away from the Arakapas Fault Zone in a previously little studied area, while the southern section is an excellently exposed section that is located directly north of the Arakapas Fault Zone (Fig. 1). We will present new field, petrographic, structural and geochemical data for both the N-Troodos and the S-Troodos sections and then compare and discuss the two data sets in terms of alternative spreading and transform processes. This approach yields valuable results and suggests that similar, but larger scale studies of this type would be worthwhile for the Troodos and other ophiolites.

In addition, we also present some new data concerning a possible extension of the Arakapas Fault Zone, which is now preserved as a serpentinite-dominated lineament within the Late Cretaceous Moni Mélange in south-central Cyprus (Fig. 1). This provides new evidence of sea-floor exposure of ultramafic rocks in Cyprus.

NORTH-TROODOS SECTION

Fieldwork was carried along a previously undescribed road-cut that extends for ~16 km NW-SE (as the crow flies) from south of the towns of Lefka to near Pano Pyrgos (Figs. 1, 2). The road is extremely sinuous and winds in and out of steep-sided valleys for a total distance of ~ 40 km. Exposure is excellent where the road cuts ridges but diminishes in the valleys and generally in the west of the section. The most prominent geomorphological feature is the Xeros river valley which runs northwards across the road transect, to the west of Lefka. Although mostly exposing sheeted dykes the road twice winds northwards into the overlying Troodos extrusive series.

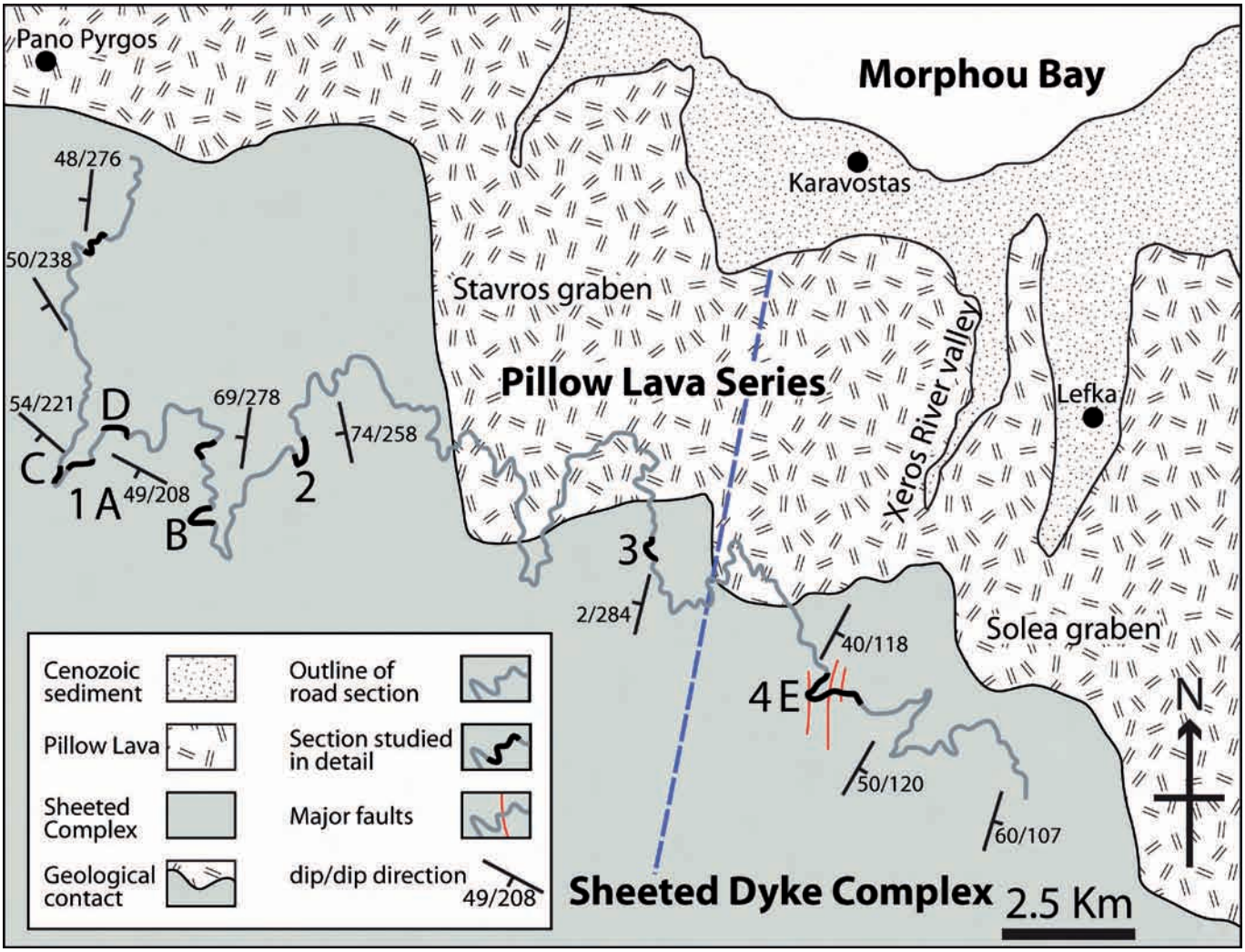

Fig. 2 - Simplified geological map of the area studied along the northern margin of the Troodos Massif (see Fig. 1). The sinuous Pyrgos road section is indicated. Calculated average dip and dip directions of the sheeted dykes are indicated for different segments of the road section (nos. 1-4). Note the change from easterly dipping dykes in the east, to westerly dipping dykes in the centre and west of the transect. The boundary between the two domains (broken line) is correlated with the boundary btween the Stavros and Solea Grabens (see Fig. 1).

The specific aims of the fieldwork along the northern margin of the Troodos ophiolite were:

1. To investigate the possible relationships between faulting and magmatism; 2. To determine whether there is any sequential organisation in the different types of dyke present; 3. To investigate any possible chemical trends in the composition of the intrusions relative to the types of intrusive rocks and their relative timing of emplacement; 4. To carry out a reconnaissance of the structure of the sheeted intrusive rocks to determine any large-scale trends in the orientation of the dykes and to compare any such trends with better documented intrusive domains to the east (e.g., Solea Graben).

Observations were made of the relative chronology (i.e. cross-cutting relationships) of dykes of lithologically different character, focusing on representative, well-exposed outcrops. This involved making detailed sketches (with corresponding photographs) and recording dyke width and colour, dyke lithology, degree of alteration, faulting, nature/style of intrusion, mineralogy, crystal-size and the type and degree of alteration.

To provide a basic structural framework, the angles of dip and the direction of dip of the dykes were measured systematically approximately every 200 m along the road section, where exposed. This revealed great local variation in dyke orientation. To reveal any overall trends, the local dip measurements were then averaged and plotted for every few kilometres along the road section, as shown in Fig. 2. This revealed overall trends in the orientation of the dykes, comparable with previous studies of the sheeted dykes in adjacent areas (e.g., Moores et al., 1990). However, no attempt was made to carry out a detailed study of the three-dimensional structure of the sheeted complex along the road section.

DYKE LITHOLOGIES

Representative intervals of the road section were studied in detail, ranging in length from 40 m to 300 m (see 1-4 in Fig. 2). Four distinct types of intrusion, in the form of epidotised dykes, diabase dykes, gabbro, or plagiogranite were recognised within these sections. The dyke types are described below in order of the relative age of intrusion based on crosscutting relations.

1. *Epidotised dykes*.

These form ~ 18% (by number) of the sections studied in detail. These dykes are characteristically dark green to yellowish and strongly altered to quartz, epidote, calcite, pyrite and hematite, with secondary alteration minerals (e.g., malachite). Hydrothermal alteration typically affects some of the dykes within a zone of intense alteration, which is commonly bounded by faults or less altered dykes (Fig. 3a, b). In some cases the dykes have been largely altered to quartz or epidosite, such that chilled margins and thus the dyke contacts are obscured. Individual pyrite crystals within hydrothermally altered zones are up to 7 cm in size.

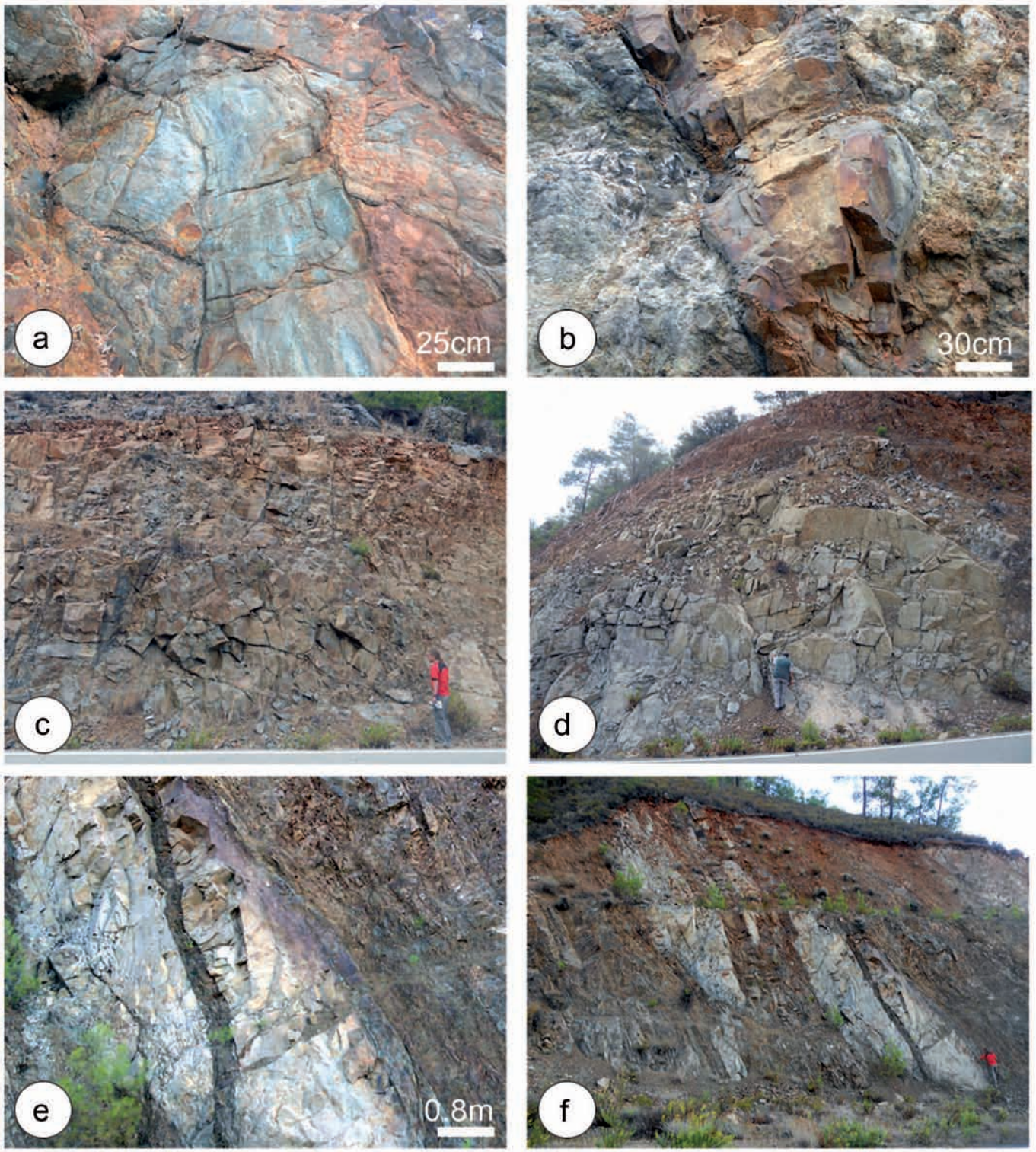

Fig. 3 - Field photographs of intrusive relations from the north-margin transect. a- Epiditotised sheeted dykes. Highly mineralised dyke material forms a triangular inclusion in lower left of photograph, cut by steep mineralised dykes (centre), viewed eastwards; b- Strongly mineralised interval in which dykes are scarcely recognisable (right and left), cut by an unmineralised (but altered) steep dyke (centre) (viewed southeastwards); c- Sill-like body of microgabbro, possibly created by localised magma ponding (C. Xenophontos, personal communication, 2011) (viewed northwestwards); d- Fault-offset gabbro intrusion (viewed southwestwards); e- Steeply dipping plagiogranite dyke (pale) cut by a small, relatively unaltered late-stage diabase dyke (viewed eastwards); f- Steeply inclined plagiogranite (pale) cut by later sub-parallel diabase dykes (viewed southwards).

2. *Gabbroic intrusions*.

There are numerous examples, especially in the east of the section, of medium to coarsely crystalline pale-coloured gabbroic bodies, individually > 5 m wide (Fig. 3c, d). The gabbros are mostly made up mostly of pyroxene, olivine, plagioclase and oxide minerals (e.g., magnetite); they make up ~ 4% of the recorded dykes. The gabbroic bodies exhibit variable intrusive relations, ranging from large intrusions, tens of metres across (often lacking exposed chilled margins), to others that are of similar thickness to many of the diabase dykes (< ~ 3 m). In one case, a medium to coarse-grained gabbro body appears to represent a sill-like intrusion (C. Xenophontos, personal communication, 2011).

3. *Diabase dykes*.

These are the most common type of intrusion, making up ~ 57% of the dykes overall (Fig. 3e; right-hand side of photograph). The dykes are fine to medium grained with a characteristic greyish colour. Some examples contain porphyritic clinopyroxene set in a groundmass of plagioclase, pyroxene, amphibole and oxide minerals. The diabase dykes range in thickness from 0.52 m to 3.6 m, with an average ~ 1.7 m.

4. *Plagiogranite dykes*.

These comprise ~ 9% of the sections studied (see 1-4 in Fig. 2) and are easily recognisable based on their distinctive pale yellow/beige colour and typical mineralogy of plagioclase, amphibole, minor quartz and oxide minerals (Fig. 3e, f). The plagiogranite dykes have a typical thickness of 1-2 m and are nearly always relatively fine grained.

5. *Late-stage diabase dykes*.

Although quite numerous, this type of dyke accounts for only ~ 12% of the total thickness of the sheeted intrusive complex in the sections studied. These dykes cut all of above types of intrusion and also many of the N-S trending faults. The dykes are thin (mostly < 1 m; see Fig. 3e), commonly sinuous and are typically injected into zones of structural weakness, for example along faults, zones of porous fault breccia, or dyke margins. These relatively late-stage dykes are fine grained and include pyroxene, olivine and a higher percentage of opaque oxide minerals than the other dyke types, based on thin section analyses. Quartz-filled amygdales are abundant in some cases. Where weathered, these dykes are reddish brown.

REGIONAL-SCALE STRUCTURE

The relative numbers of dykes of different orientations that are exposed along the north margin (Pyrgos) road section are shown in Fig. 4 (see 1-4 in Fig. 2). In general, the

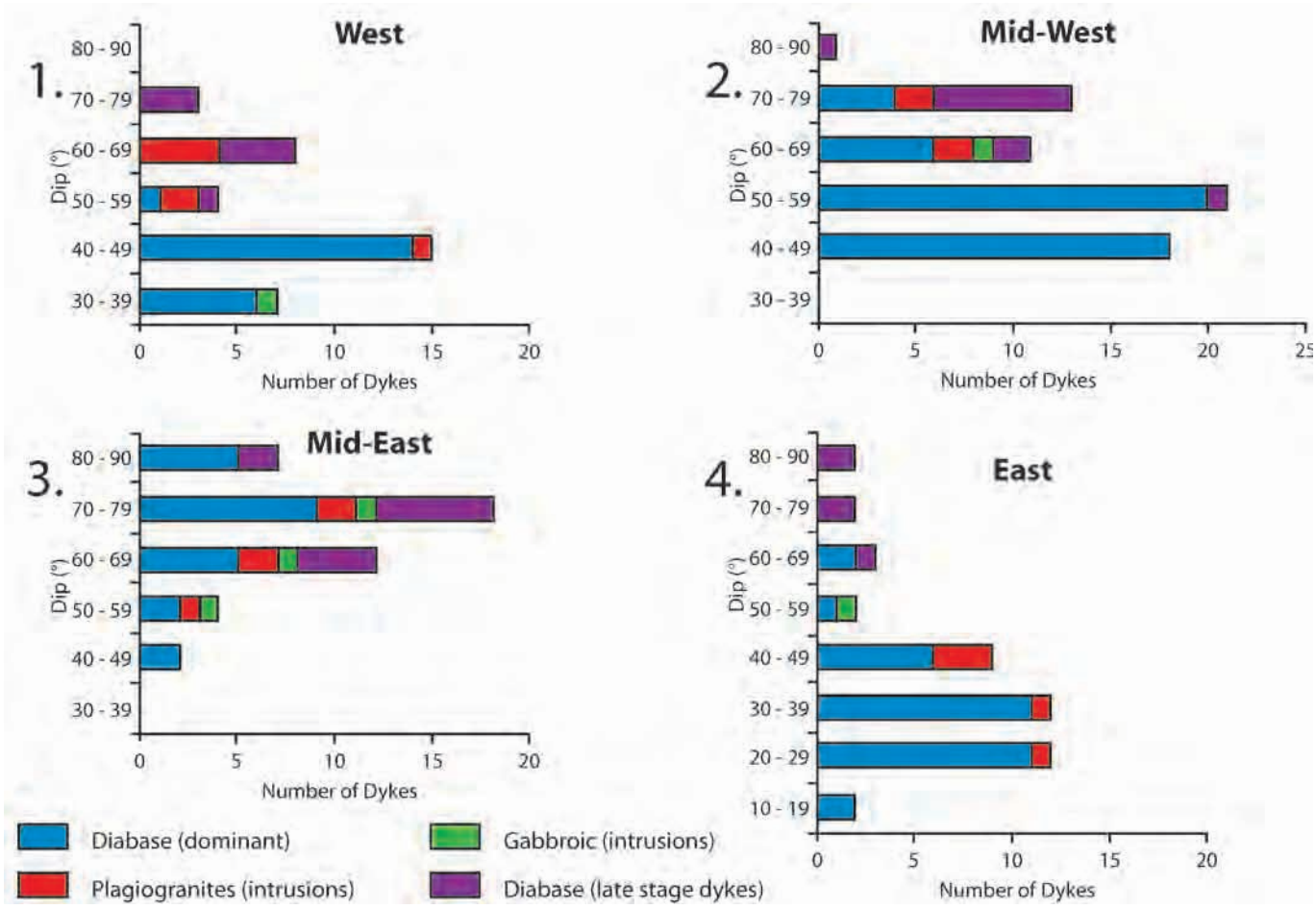

Fig. 4 - Measured orientations of sheeted dyke suites (dip and dip direction) at four representative locations along the road section (see Fig. 2 for locations 1-4). The dykes are rotated to generally lower angles in the east, compared to the western part of the Stavros Graben. The plots also highlight the relatively late-stage nature (i.e. steep dips) of the gabbro intrusions. The plagiogranites also appear to be relatively late-stage intrusions (also steeply dipping), and are cut by variably inclined diabase dykes.

plagiogranites and the late-stage diabase dykes tend to be more steeply inclined than the earlier-stage diabase dykes.

In the east, the section is cut and offset by three prominent shallow-dipping ESE and NNE-trending faults (see Figs. 2, 3a). The largest of these faults is characterised by a > 10 m-wide zone of brecciation (Fig. 5b), in which the hanging wall of the main fault plane exhibits a 3-4 m-thick shear zone above the footwall. Two additional faults occur structurally above this but with a smaller thickness of fault breccia (~ 2 m) (Fig. 5c).

The ~ NNE-SSW-trending broken line in Fig. 2 separates two different parts of the road section in which the dykes dip in different directions and at different angles. The dykes in the east dip eastwards at relatively shallow angles, whereas the dykes to the west dip westwards at generally steeper, but variable angles. The precise contact between the differently dipping dyke domains is unfortunately not exposed in the road section.

Comparison with previous mapping of the periphery of the Troodos Massif further north and northeast (Moores et al., l990; Fig. 1) indicates that the eastward-dipping dykes can be correlated with the well-documented Solea Graben (Fig. 1). The three major low-angle faults, together form part of the western margin of this important structural domain. The crust further west is correlated with the less well-known Stavros domain or graben of Moores et al. (l990); beyond this, the little-known Pomos domain extends to the west coast of the island. Previous mapping of the Solea Graben to the south of the Pyrgos road section, in the vicinity of the Troodos plutonic complex has revealed the presence of a large extensional fault (Troodos Forest Fault; to the south of Fig. 2) that is believed to have been active during seafloor spreading (Hurst et al., l994). This fault, or an equivalent, may extend northeastwards and link up with the major extensional detachment fault zone that separates the Solea and Stavros spreading domains in the Pyrgos road section.

Within the Stavros Graben, the dykes initially dip at 70° to 82° towards the west (Fig. 2). In the west, where the outcrop is better, the dykes dip at variable but commonly shallower angles to the west (48° to 85°). In the far northwest, the road transects a sheared outcrop of sheeted dykes with screens of pillow lava that is correlated with the traditional Basal Group of the Troodos Lava Series. Finally, near Pano Pyrgos, the road traverses poorly exposed, weathered pillow lavas that are correlated with the traditional Lower Pillow Lavas of the Troodos Lava Series (Wilson and Ingham, l959).

Two main sets of steeply dipping extensional faults are recognised along the section studied, one trending parallel to the average ~ N-S trend of the dykes and a second trending ~ E-W (e.g., see Fig. 5d). The majority of the ~ N-S faults along the road section are assumed to be contemporaneous with the Late Cretaceous genesis of the Troodos ophiolite, although some N-S steep faults are known to exist within the Cenozoic sedimentary cover, as exposed along the northern margin of the Troodos Massif (Kinnaird and Robertson, 2013). The ~ E-W faults lack evidence of associated magmatism and are assumed to postdate sea-floor spreading. Comparable ~ E-W steep faults (62°-90°) cut the sedimentary cover along the northern margin of the Troodos Massif to the east of the study area (Kinnaird and Robertson, 2013, and references therein).

Many of the N-S-trending extensional faults (dipping at 22°-85°) show evidence of multiple phases of extensional faulting (Fig. 5e, f). For example, well consolidated, hydrothermally altered fault breccias are, in places, cut by faults that are associated with a younger set of unmineralised and unconsolidated fault breccias. Some of the extensional faults are intruded by dykes, which were themselves cut by later dykes, with similar or different orientations.

Five local sections that illustrate low-angle dykes and complex crosscutting relations were studied in detail, as shown in Fig. 6A-E (see Fig. 2 for locations). The location of samples that were chemically analysed (LM numbers) are also indicated.

Assuming that the dykes were intruded vertically, the measured angle of a sheeted dyke is an indication of the amount of rotation about a horizontal axis that has taken place since intrusion. Where repeated dyke intrusion has taken place, as seen within individual outcrops, successive rotations to lower angles can be inferred. It should be noted, however, that the relative chronology of dyke intrusion can only be inferred within individual intact sections. Inferences about the relative timing of dyke intrusion cannot be made for exposures that are separated by through-going faults, for which the offsets cannot be determined, in areas of poor exposure or for the entire section of sheeted dykes (in the absence of palaeomagnetic data or absolute age data).

In Fig. 6A, the oldest event locally was the emplacement of the protoliths of the epidosite dykes (lower right). Where rarely observable, dip angles range from 34° to 38° (towards 224° to 249°). An additional, wedge of epidosite occurs to the left of the epidosite dykes. The main epidosite unit was later cut by four diabase dykes dipping from 54° to 60° (towards 252° to 258°), and then by a plagiogranite dyke with chilled margins and a steeper dip (72° towards 264°). The fault that separates the right and left sides of the local section appears to cut diabase and epidosite but does not affect the plagiogranite or the youngest dykes that are chilled against the plagiogranite. Both the plagiogranite and the late-stage dykes appear to have exploited weakness within the fault zone and step around an obstacle beneath. To the left of the fault, the section is largely composed of diabase, dipping at angles of 43° to 50° (towards 216°-243°). In addition, there are several crosscutting features: a plagiogranite dyke (dipping at 62° towards 256°) and several dykes from the late-stage suite, of which two exhibit injection into a fault plane (dipping at 69° towards 253°). Two steeper dipping dykes show snake-like intrusion patterns (dipping at 72° towards 243° and at 82° towards 293°).

In Fig, 6B, a striking feature is a large gabbroic intrusion (> 10 m thick) with no observable chilled margin. A sheared contact with diabase dykes dips at an angle of 55° towards 258°; this appears to postdate the gabbro intrusion. The diabase dykes dip at up angles of up to 64°. A single plagiogranite dyke (dipping at an angle of 69° towards 278°) cuts the diabase and also a fault that itself cuts the diabase. In addition, several diabase dykes cut both the gabbro and the diabase at higher angles (64° to 78° towards 258°-280°) than the dykes that cut the plagiogranite. The youngest dyke (furthest left) appears to have utilised weaknesses (possibly the adjacent fault) to facilitate upward magma injection.

Fig. 6C reveals that the oldest event locally was the intrusion of diabase dykes that were transformed to epidosite. Remnant dykes are seen to dip at angles of 34°-38°, towards 238°-248°. One epidosite dyke remnant appears to lie within a poorly exposed gabbroic intrusion, dipping at an angle of 32° to 224°, suggesting an even earlier intrusive history. Crosscutting diabase dykes dip at angles between 34° and

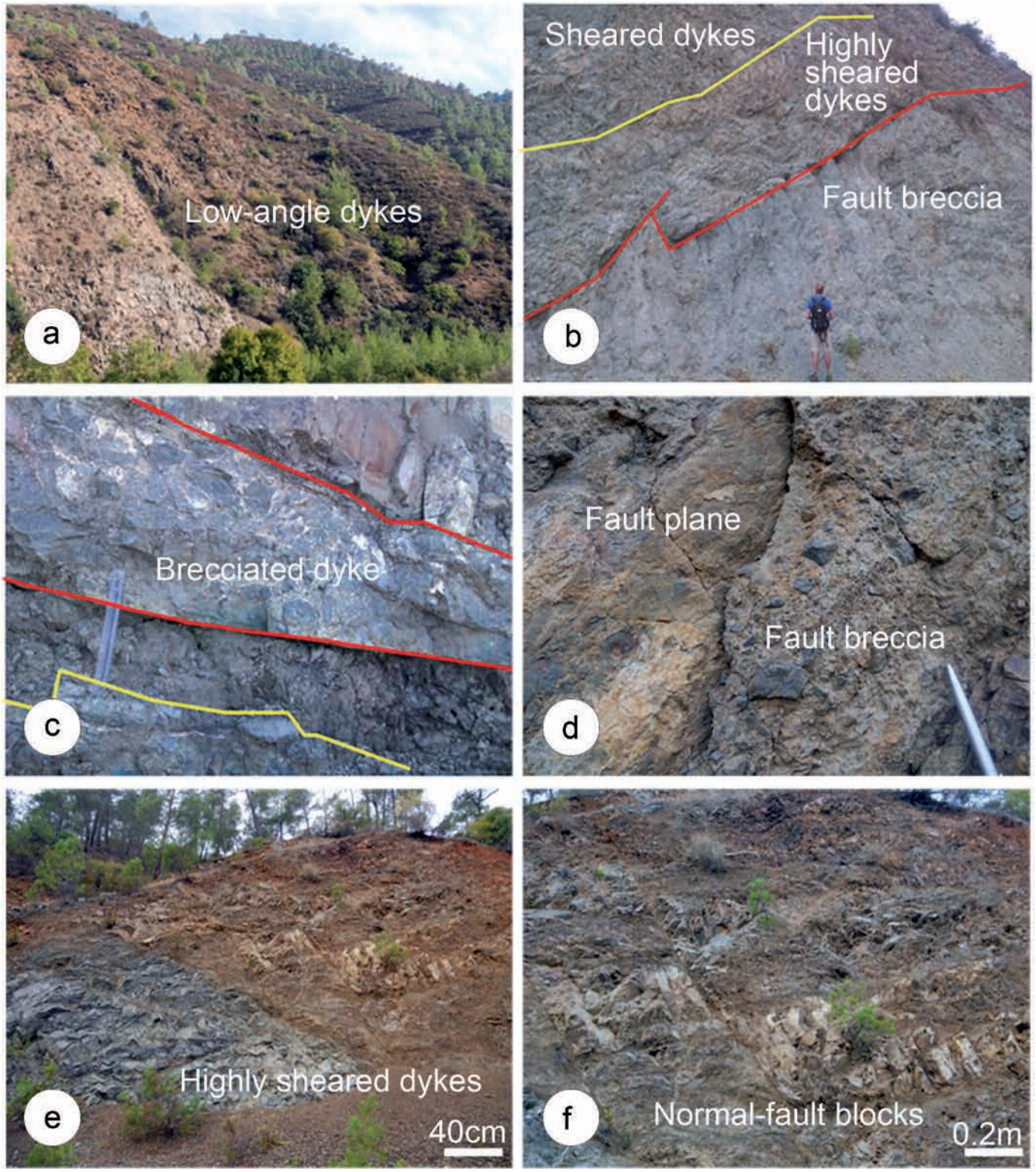

Fig. 5 - Field photographs of fault geometries along the north-margin transect. a- Large area of eastward-rotated sheeted dykes in the westernmost part of the Solea Graben (viewed eastwards); b- Contact zone between the Solea Graben (to the east; looking eastwards) and the Stavros Graben to the west. A thick fault breccia zone is overlain by highly sheared dykes and then by less sheared dykes; near the Xeros River (viewed southwards); c- Rotated dyke that has been brecciated (between the parallel solid lines), with sheared dykes above. This fault zone is hydrothermally altered and veined. Later faulting has given rise to poorly fault breccia (below irregular solid line) (30 cm ruler for scale) (viewed southeastwards); d- Steeply inclined ~ E-W fault marked by fault breccia and slickensides. Such faults are interpreted as the result of normal faulting that post-dated post-sea spreading (viewed southwestwards); e- Extensional shear zone within sheeted dykes of the Stavros Graben. The throw on the lower fault is larger than the scale of the outcrop and thus cannot be measured. The colour variation reflects differences in weathering rather than lithological differences (viewed westnorthwestwards); f- Detail of the upper part of c. Dykes have been rotated to a low angle and then cut by later, small-scale high-angle faults (viewed westnorthwestwards).

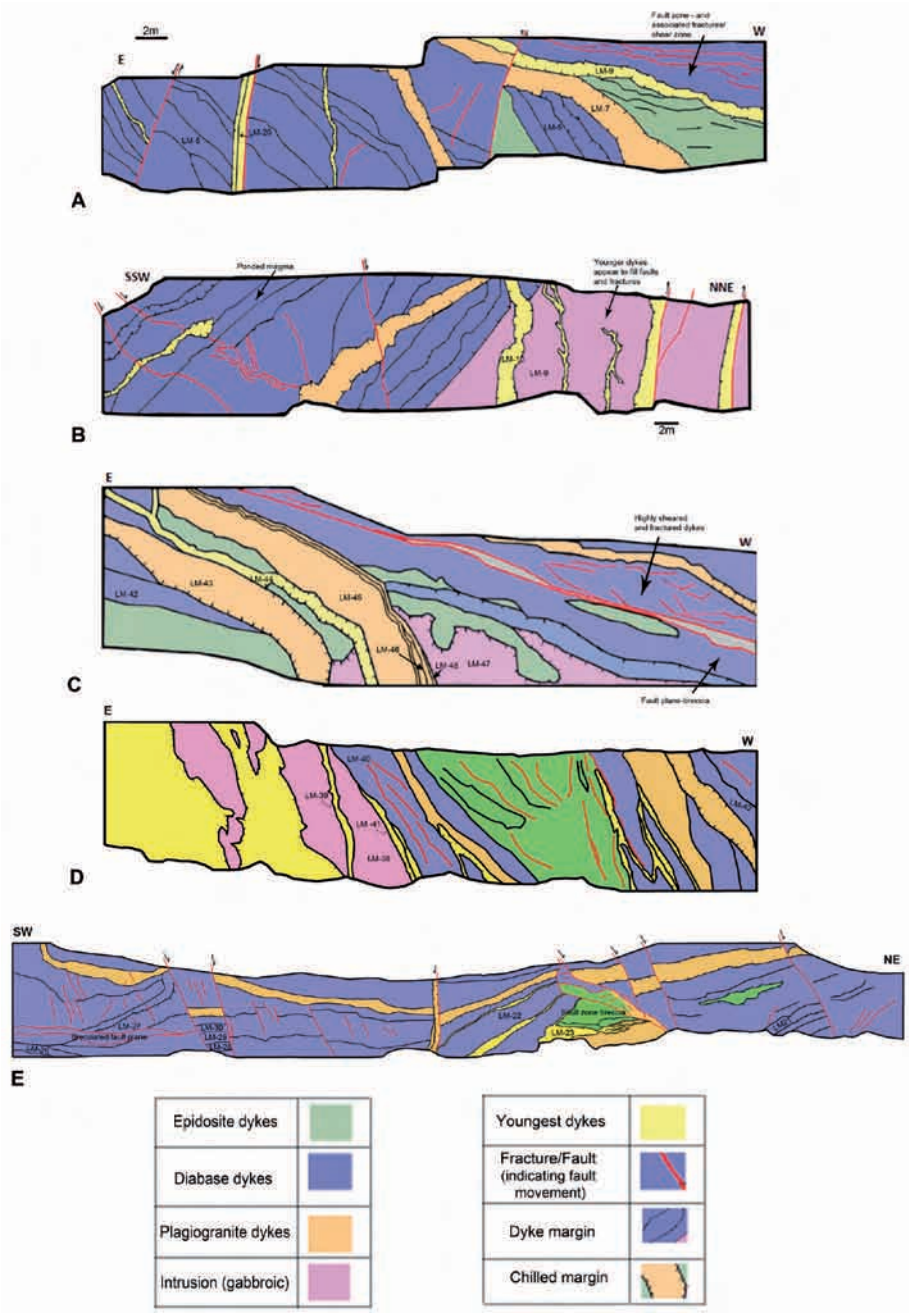

Fig. 6 - A-E. Representative examples dyke relationships, as exposed in the N-Troodos (Pyrgos) road section. See Fig. 2 for the locations of A-E and the text for explanation. The drawings show the relative timings of emplacement of different types of intrusion in different parts of the N-Troodos road section. Samples that were analysed are numbered (see Fig. 14). The interpretation of each of the drawings is explained in the text. GPS WGS 84/UTM A - 473530/3883555; B - 473545/3883618; C - 471433/3884468; D - 471401/3884455; E - 471304/3884428.

42°, towards 224° to 247, showing that, in this case, little relative rotation has taken place between the epidosite, the gabbro and the diabase intrusions. The diabase dyke in contact with the gabbroic intrusion appears to lack a chilled margin, probably because the gabbro was still hot when intruded. However, a chilled margin is present where the dyke intrudes diabase dykes. Plagiogranite and the youngest suite of dykes show similar dips and crosscut everything in this part of the section. Two dykes (LM 46, LM45 and LM47) cut the plagiogranite. A large zone of fault breccia (up to 1 m in thick) dips at an angle of 34° (towards 240°), as seen in the upper levels of this section. A 1-3 m-wide interval above the fault plane is represented by highly sheared dykes (dipping 40° to the SW).

In addition, Fig. 6D illustrates a relatively early epidotised dykes, cut by later dykes and then by relatively late-stage plagiogranite. The large plagiogranite intrusion in the left of the section is cut by fine-grained basaltic dykes.

Finally, Fig. 6E illustrates dykes, which are mainly near horizontal, cut by relatively high-angle faults. There is a small remnant of relatively early epidotised dykes in the right of the section. Dykes of two different generations were apparently rotated together to a low angle and then cut by a narrow high-angle dyke.

TECTONIC INTERPRETATION

Taken, together the observations from the road section as a whole and the detailed information from the five sections (Fig. 6) indicate the following overall relative timing of intrusion:

1. Zones of epidotised dykes that occur as dykes, wedges and areas around fractures represent early-stage intrusion in all cases. These highly altered dykes are commonly at a relatively low angle, intensely sheared and cut by less altered, less deformed higher-angle dykes.

2. The larger gabbroic intrusions represent relatively early intrusions that are chilled against diabase or epidosite and are frequently cut by plagiogranite and by younger crosscutting dykes.
3. The predominant diabase dykes vary in dip. Swarms of similarly orientated dykes (typically with > 10s of dykes in each package) commonly crosscut each other.
4. The plagiogranites are observed to crosscut epidosite and also the majority of the diabase dykes.
5. The thin, sinuous, commonly brown-weathering fine-grained dykes postdate all the other types of dyke.

The systematic nature of these phases of intrusion provides a basis for chemical comparison.

GEOCHEMISTRY

The major and trace element composition of dykes from the selected segments of the road section (1-4 in Fig. 2) was determined by X-ray fluorescence using a previously described method (Fitton and Goddard, 2004; Fitton et al., l998; see Tables 1 and 2). The specific aims of the geochemical study were as follows: 1. To determine if there is any systematic chemical variation between the different types and phases of dyke intrusion, as summarised above; 2. Specifically, to determine if there are any overall geochemical differences between the relatively early, as opposed to relative late diabase dykes, where these could be determined from crosscutting relations; 3. To determine if any overall chemical differences or trends exist along the Pyrgos road section from east to west, specifically related to the Solea Graben in the east and the Stavros Graben in the west.

Care was take to collect the most visibly unaltered and unweathered samples for chemical analyses.

The samples were initially studied in thin section to indicate their suitability for analysis. The highly altered early-stage dykes contain epidote, calcite, pyrite, hematite and commonly, also secondary malachite. The hydrothermally altered rocks were not chemically analysed in view of their strong alteration. The typical grey diabase dykes exhibit porphyritic clinopyroxene set in a groundmass of plagioclase, pyroxene, amphibole plus minor amounts of oxide minerals (e.g., magnetite). The gabbroic intrusions comprise pyroxene, olivine, plagioclase and also oxide minerals (e.g., magnetite). The plagiogranite dykes have a typical mineralogy of plagioclase, amphibole, quartz and minor oxide minerals. The late-stage finely crystalline dykes contain pyroxene, olivine and a notably higher percentage of opaque oxide minerals compared to the other types of diabase dyke. This may explain their tendency to weather to a deep brown colour.

In general, the dykes have undergone seafloor metamorphism of upper greenschist to amphibolite facies, coupled with varying degrees of alteration, as described from other exposure of the Troodos sheeted complex (e.g., Richardson et al., l987; Bednarz and Schmincke, 1989; Gillis and Robinson, 1990; Kelley et al., l992).

The interpretation of the chemical data hinges on the use of major and trace elements that are well established as being relatively immobile under conditions of seafloor metamorphism and surface weathering (e.g., Pearce and Cann, l973; Pearce, l975; l996).

The data were initially plotted on a rock classification diagram that utilises immobile elements (Fig. 7a). This shows that the analysed dykes lie within the field of tholeiitic basalt.

The data set as a whole can most easily be compared using MORB (mid-ocean ridge)-normalised spider dagrams (Fig. 8A-B). When the data are plotted as relatively low-angle (relatively early stage) versus high-angle (commonly later stage) dykes the high-angle dykes are on average relatively Ti-poor, although the Ti content is gradational overall between the two dyke types of different orientation. Many of the samples show a small negative Nb anomaly in the spider plots (relative to adjacent elements) which is suggestive of a subduction influence on magmatism (e.g., Pearce et al., l984).

The data were also plotted on several widely used diagrams that disciminate the tectonic settings of basalt genesis. These diagrams are applicable to sheeted dykes but not to the more coarsely crystalline or fractionated gabbros and plagiogranites, which were not analysed.

The Ti vs Zr diagram (Fig. 9), the Zr/Y vs Zr diagram (Fig. 10), Cr vs Y diagrams (Fig. 11) and the Y vs Ti diagram (Fig. 12) highlight the subduction-influenced nature of the dykes. On the Zr/Y vs Zr diagram (Fig. 10), the high-angle diabase dykes tend to be magmatically depleted, compared to the lower angle dykes. A similar trend is seen on the Cr vs Y diagram (Fig. 11), on which some of the high-angle dykes again plot in the boninite field. The TiO_2 vs MnOx10 vs P_2O_5 diagram (Fig. 13) highlights the presence of strongly depleted basalts (Mullen, l983), with many examples of both the low-angle dykes and the high-angle dykes plotting in the boninite field.

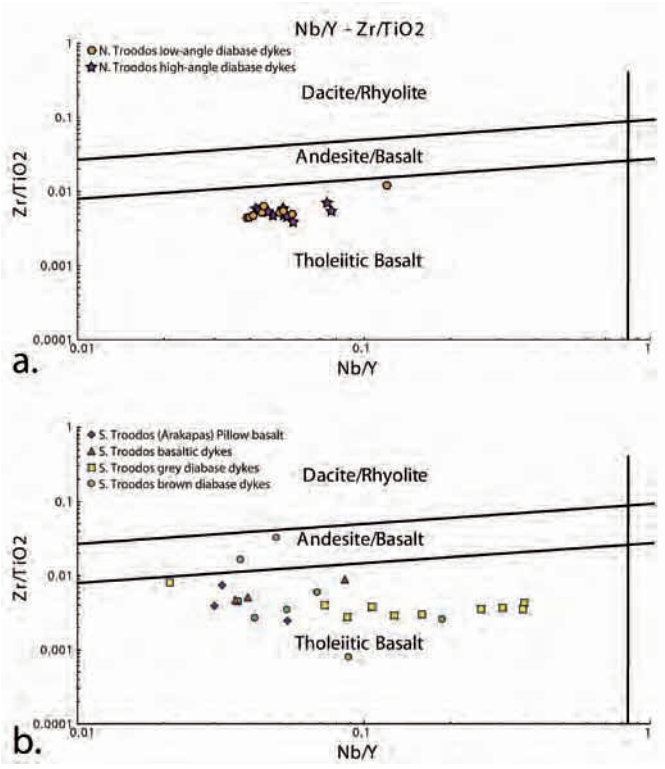

Fig. 7 - Zr/TiO_2 vs Nb/Y rock classification diagrams. a- North-Troodos (Pyrgos) section divided into relatively early-stage low-angle dykes and relatively late-stage high-angle dykes; b - South-margin section (north of Arakapas Fault Zone) divided into relatively early-stage grey dykes and relatively late-stage brown dykes. Basalt and relatively fine-grained basaltic dykes are also shown from near the southern end of the section, within the Arakapas Fault Zone. Diagram modified after Pearce (1996).

Table 1 - X-ray fluorescence data for lithologies from the north-Troodos (Pyrgos) transect.

Sample No. Rock Type	LM-5 Diabase	LM-6 Diabase	LM-17 Diabase	LM-21 Diabase	LM-22 Diabase	LM-28 Diabase	LM-29 Diabase	LM-30 Diabase	LM-42 Diabase	LM-7 Plagiogranite	LM-11 Plagiogranite	LM-40 Plagiogranite	LM-43 Plagiogranite	LM-45 Plagiogranite
SiO2	57.48	53.40	56.24	53.25	50.24	59.44	54.08	56.52	58.27	70.12	62.11	59.73	69.58	53.06
TiO2	0.73	0.47	0.51	0.59	0.37	0.69	0.54	0.67	0.75	0.42	0.75	0.81	0.49	0.77
Al2O3	14.64	16.35	15.50	15.51	20.83	14.75	15.60	15.47	14.08	13.48	13.90	14.14	13.15	16.59
FeO	12.20	9.25	8.04	16.49	9.59	11.98	10.09	11.21	11.51	4.98	11.62	12.17	6.30	11.61
MnO	0.23	0.20	0.17	0.20	0.16	0.19	0.16	0.23	0.20	0.10	0.08	0.17	0.09	0.20
MgO	4.23	6.81	6.45	4.74	5.41	4.21	5.82	5.69	3.73	0.77	2.14	3.04	1.27	5.32
CaO	3.71	7.61	4.09	2.53	10.38	4.21	6.48	6.34	5.10	2.99	3.14	1.98	2.05	3.05
Na2O	3.00	2.44	5.25	2.25	1.41	3.03	1.67	2.64	3.80	5.07	3.48	3.66	5.47	5.83
K2O	0.01	0.41	0.01	0.24	0.22	0.62	0.48	0.47	0.26	0.03	0.15	0.03	0.01	0.03
P2O5	0.04	0.03	0.03	0.05	0.02	0.05	0.03	0.04	0.04	0.07	0.07	0.05	0.07	0.04
LOI	3.27	2.73	3.20	3.74	0.96	0.00	4.56	0.00	1.85	1.60	2.43	3.74	1.16	3.27
Total	99.54	99.70	99.50	99.60	99.59	99.17	99.52	99.27	99.59	99.63	99.89	99.88	99.78	99.77
Sr	69.4	111.1	46.1	59.6	98.3	89.7	37.1	88.7	98.5	69.2	106.3	58.9	56.3	72.1
Rb	0.1	1.7	0.1	1.4	1.3	2.6	1.9	2.3	1.8	0.2	0.9	0.3	0.1	0.4
Ba	6.1	13.6	1.2	6.8	8.9	12.3	4.9	10.9	11.2	4.0	3.4	4.6	3.1	7.7
Nb	0.9	1.7	0.7	0.7	0.4	0.9	0.7	0.7	0.8	1.7	1.4	1.0	1.5	0.8
Ce	3.7	3.4	3.4	1.6	2.0	4.3	3.9	3.5	2.8	7.6	7.7	4.6	6.0	5.4
Zr	36.5	57.8	27.1	38.1	16.7	38.6	28.6	32.1	34.1	57.8	55.7	38.8	53.9	37.7
Y	16.0	14.2	13.8	15.7	10.2	17.2	15.9	17.1	20.2	24.6	26.8	18.3	25.1	18.6
Zn	202.8	107.1	139.4	87.7	68.9	70.7	97.0	71.7	123.5	153.8	31.3	72.7	33.4	125.6
Cu	1586.5	44.7	8.1	774.5	88.5	27.7	148.1	8.4	91.7	35.4	238.6	888.8	196.6	175.8
Ni	24.7	39.8	47.5	79.2	81.8	15.2	27.1	19.5	13.4	5.6	8.9	13.7	5.3	26.7
Cr	13.0	23.9	93.4	126.4	129.7	9.1	22.5	11.2	9.4	12.3	13.4	10.6	8.0	19.3
V	459.8	242.9	243.1	307.5	253.9	374.3	276.1	331.1	348.2	18.0	147.4	379.5	47.5	460.6
Sc	44.1	44.5	43.1	46.9	42.2	43.7	36.9	54.6	49.1	15.4	30.0	43.5	21.7	51.1
La	n.d.	0.7	60.2	n.d.	n.d.	0.6	n.d.	n.d.	n.d.	1.0	0.3	n.d.	0.3	1.0
Nd	2.8	3.0	2.4	2.8	2.9	4.2	2.3	3.2	3.2	7.1	5.6	4.0	5.5	2.6
U	0.2	n.d.	0.0	0.5	n.d.	0.0	n.d.	0.0	0.0	0.2	0.4	0.2	0.2	0.0
Th	0.5	0.3	n.d.	n.d.	0.3	0.4	0.3	0.7	0.2	0.1	0.2	0.5	0.1	n.d.
Pb	n.d.	1.0	0.1	0.7	0.3	0.1	1.0	0.1	1.0	1.0	0.5	n.d.	0.1	0.2

n.d. = not detected.
Major elements in wt.% oxide; trace elements in parts per million (ppm).

Table 2 - X-ray fluorescence data for additional lithologies from the north-Troodos (Pyrgos) transect.

Sample No.	LM-9	LM-38	LM-47	LM-8	LM-10	LM-16	LM-20	LM-23	LM31	LM-39	LM-41	LM-44	LM-46	LM-48
Rock Type	Gabbro	Gabbro	Gabbro	Young Suite	Young Suite	Young Suite	Young Suite	Young Suite	Young Suite	Young Suite	Young Suite	Young Suite	Young Suite	Young Suite
SiO2	50.77	56.85	69.73	58.02	47.05	54.75	51.00	57.13	60.17	50.76	56.63	52.90	53.49	57.47
TiO2	0.21	0.69	0.43	0.62	0.40	0.37	0.30	0.45	0.76	0.64	0.79	0.27	0.28	0.64
Al2O3	19.16	14.90	13.38	15.38	11.90	15.28	12.18	15.57	15.47	17.61	14.14	12.10	12.56	14.63
FeO	6.51	10.42	6.59	9.26	5.70	7.98	8.24	8.15	9.99	11.82	12.45	7.76	8.26	10.51
MnO	0.14	0.16	0.07	0.21	0.13	0.18	0.15	0.14	0.19	0.16	0.23	0.16	0.25	0.18
MgO	7.33	5.20	0.75	5.21	4.21	8.25	13.84	8.20	3.99	6.22	3.44	10.62	9.57	3.53
CaO	11.05	3.85	1.29	2.39	4.85	4.45	7.85	4.49	5.75	2.02	3.76	6.05	7.00	4.91
Na2O	2.17	4.06	6.13	5.32	4.97	4.99	1.75	5.21	2.61	5.51	3.45	3.10	3.37	4.40
K2O	0.30	0.26	0.02	0.02	0.03	0.02	0.22	0.31	0.13	0.39	0.02	0.13	0.05	0.02
P2O5	0.01	0.04	0.08	0.04	0.02	0.02	0.01	0.03	0.06	0.03	0.05	0.01	0.02	0.04
LOI	2.03	3.27	1.06	3.11	20.30	3.28	3.85	0.00	0.00	4.27	4.74	6.20	4.82	3.46
Total	99.67	99.70	99.53	99.59	99.57	99.58	99.39	99.68	99.13	99.43	99.69	99.30	99.66	99.78
Sr	106.1	76.9	64.9	45.6	51.2	54.4	56.0	66.8	96.2	30.7	19.8	67.0	65.9	82.0
Rb	1.8	0.9	0.3	0.2	0.1	0.3	1.1	1.1	1.0	1.4	0.3	0.6	0.3	0.2
Ba	13.8	4.1	6.4	1.8	1.7	4.5	10.5	12.0	10.6	2.4	1.7	7.3	5.7	0.8
Nb	0.3	0.6	1.4	0.8	0.7	0.5	0.5	0.6	1.1	0.8	0.9	0.6	0.7	0.9
Ce	2.2	3.0	8.1	5.3	3.8	4.0	1.2	2.0	4.8	2.4	3.0	3.2	2.5	6.1
Zr	11.3	28.6	59.6	33.5	22.6	22.5	14.1	22.2	44.4	25.4	37.8	15.0	20.3	36.9
Y	7.0	16.4	28.0	17.3	16.3	11.9	9.3	11.4	21.2	14.1	18.8	7.8	9.4	17.4
Zn	51.9	74.6	57.5	402.7	44.1	149.8	71.3	51.2	87.9	109.1	82.9	86.3	129.0	86.1
Cu	4.1	37.7	691.7	156.0	1387.4	96.5	106.9	10.9	419.9	1478.8	582.0	93.6	5.9	24.9
Ni	63.5	16.6	2.9	24.1	33.3	65.1	355.2	38.4	18.6	24.7	15.4	130.3	87.7	8.5
Cr	63.2	9.6	4.8	12.4	35.3	159.7	612.9	35.6	15.5	16.6	12.4	477.8	439.2	11.6
V	162.7	344.9	33.4	310.4	269.4	224.6	195.6	209.1	329.5	434.5	441.9	205.4	234.3	398.7
Sc	37.8	49.2	19.0	45.4	43.3	44.6	31.5	40.7	46.0	49.1	43.7	41.1	46.7	43.7
La	n.d.	n.d.	1.3	n.d.	n.d.	n.d.	n.d.	0.4	n.d.	n.d.	n.d.	n.d.	0.3	0.8
Nd	1.2	3.0	7.6	3.5	2.9	1.7	0.6	2.8	5.1	2.2	3.0	1.6	1.8	3.4
U	n.d.	n.d.	0.1	n.d.	n.d.	n.d.	0.2	n.d.	0.0	n.d.	0.0	0.0	n.d.	n.d.
Th	n.d.	n.d.	0.1	n.d.	n.d.	0.3	n.d.	n.d.	0.4	0.6	0.3	n.d.	n.d.	0.2
Pb	0.2	0.8	n.d.	0.5	0.2	0.2	1.2	0.5	0.4	n.d.	n.d.	0.1	0.4	1.4

n.d. = not detected.
Major elements in wt.% oxide; trace elements in parts per million (ppm).

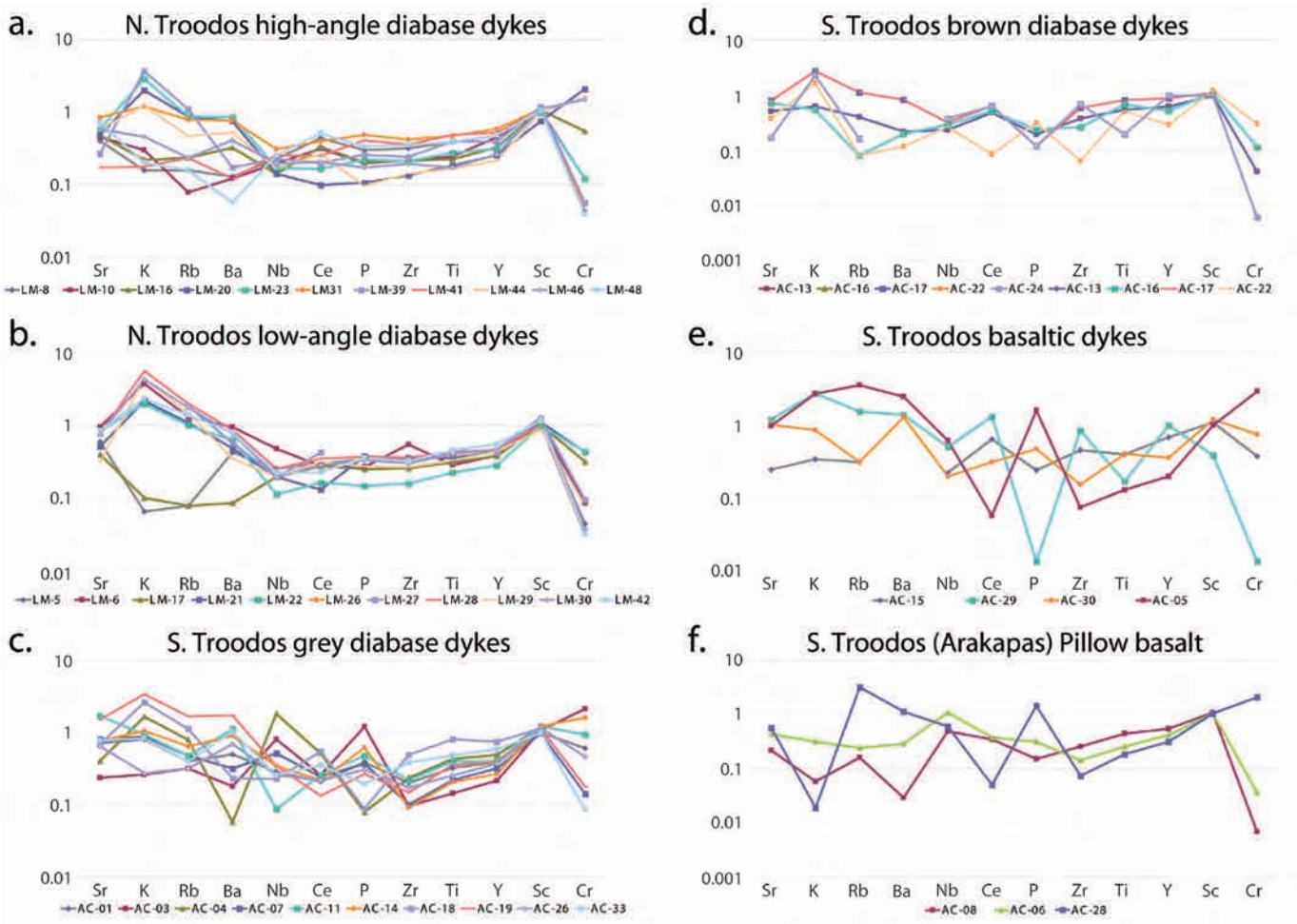

Fig. 8 - MORB-normalised multi-element spider diagrams for different mafic dyke lithologies. a-b- from the north-Troodos (Pyrgos) section), divided into relatively early low-angle dykes and relatively late high-angle dykes; c-f- from the south-margin (Arakapas) section divided into relatively early grey dykes (c), relatively late brown dykes (d), relatively fine-grained basaltic dykes (e) and basalt (f). e and f are from near the southern end of the section. Normalising values from Hofmann (1988). See text for explanation.

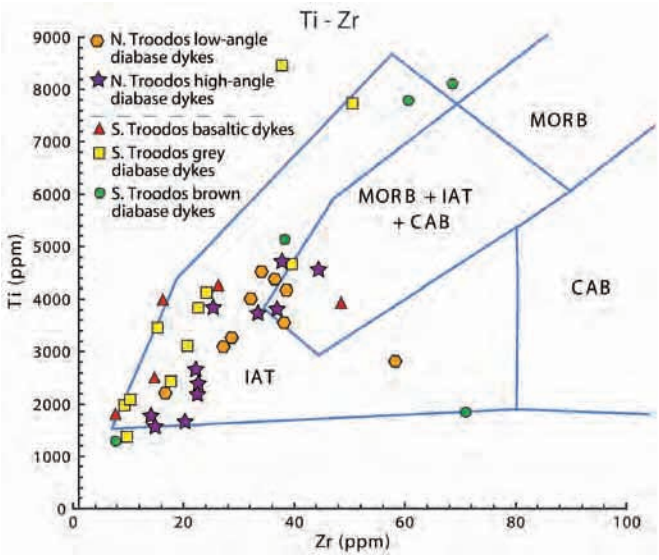

Fig. 9 - Ti vs Zr tectonic discrimination diagram (after Pearce and Cann, 1973) showing diabase dykes collected from both the northern and southern Troodos transects. Fields: CAB- Calk-alkaline basalt; MORB- Mid ocean ridge basalt; IAT- Island-arc tholeiite. See text for explanation.

To detemine if any chemical trends exist down to the level of the outcrop scale, the compositions of the crosscutting dykes in the five sections studied in detail (Fig. 6A-E) were compared, as shown Fig. 14. Of these, sections (A and C and possibly D) show overall trends from the relatively earliest to the latest basic intrusions towards relatively depleted, boninitic compositions. One section (B) shows too few cross-cutting dykes to be useful. Also, where the dykes are rotated to low angles (e.g., section E) systematic cross-cutting relations cannot be determined. In several cases, the late-stage bonintic dykes are steeply dipping (e.g., sample LM 20 in Fig. 6A). However, in other cases the boninitic dykes are significantly rotated (e.g., samples LM 45 and LM 46 in Fig. 6C).

In summary, the chemical data, based on the overall dyke attitude in the sections studied (1-4 in Fig. 2) and the more local, documented crosscutting relationships (A-E in Fig. 2) suggest that the later stage, less rotated dykes are on average more magmatically depleted, than the earlier stage, more rotated dykes. The more depleted boninite-type extrusives are inferred to have fed the upper extrusive series (Upper Pillow Lavas) of the Troodos ophiolite, which show similar chemical compositions (Pearce, l975; Pearce and Robinson, 2010).

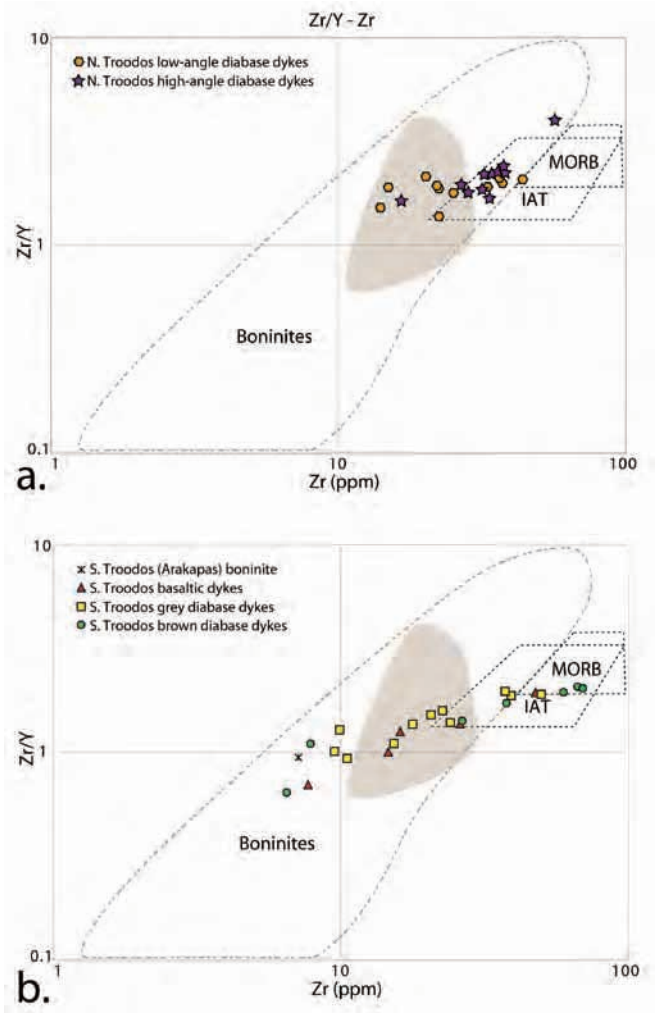

Fig. 10 - Zr/Y vs Zr tectonic discrimination diagrams (after Phillips-Lander and Dilek, 2009). a- diabase dykes from the north-Troodos (Pyrgos) section; b- dykes and basalts from the south-Troodos transect adjacent to the Arakapas Fault Zone. MORB- Mid-ocean ridge basalt; IAT- Island arc tholeiite. The shaded field represents previous data from the Arakapas Fault Zone, for comparison of the boninitic rocks (Gass et al., 1994). See text for explanation.

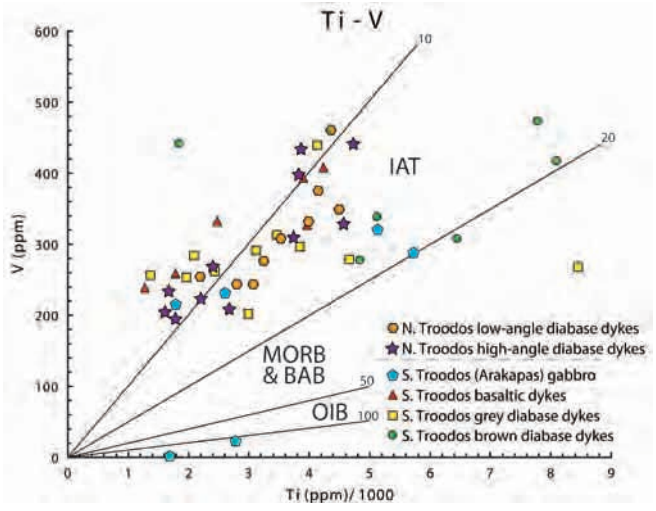

Fig. 12 - V vs Ti tectonic discrimination diagram (after Shervais, 1982). Diabase dykes from north-Troodos (Pyrgos) section (low-angle vs high-angle dykes); also dykes and basalt from the south-Troodos transect adjacent to the Arakapas Fault Zone. Fields: IAT- Island-arc tholeiite; MORB- Mid-ocean ridge basalt; BAB- Back-arc basin basalt; OIB- Ocean island basalt. See text for explanation.

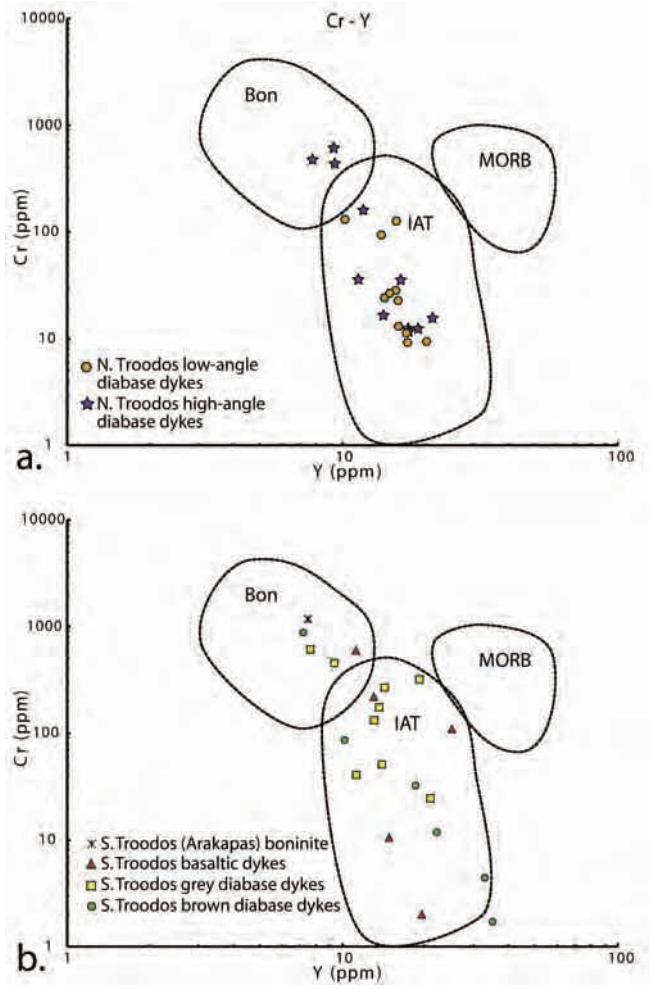

Fig. 11 - Cr vs Y tectonic discrimination diagram (Pearce, 1982). a- Diabase dykes from the north-Troodos (Pyrgos) section; b- Dykes and basalt from the south-Troodos transect adjacent to the Arakapas Fault Zone. Fields: MORB- Mid-ocean ridge basalt; IAT- Island arc tholeiite; Bon- boninite. See text for explanation.

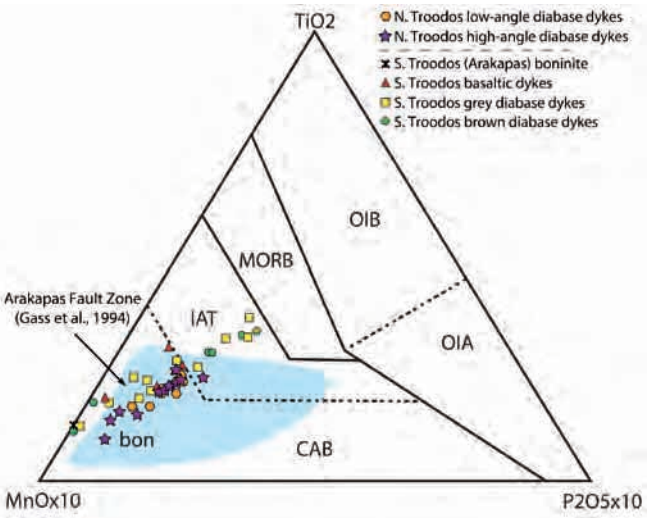

Fig. 13 - TiO_2 vs P_2O_5x10 vs MnOx10 ternary discrimination diagram (after Mullen, 1983). Diabase dykes from the north-Troodos (Pyrgos) section (low-angle vs high-angle) and dykes and basalt from the south-Troodos transect adjacent to the Arakapas Fault Zone. Fields: OIB- Ocean island basalt; OIA- Ocean island alkali-basalt; MORB- Mid ocean ridge basalt; IAT- Island arc tholeiite; CAB- Calk-alkaline basalt; Bon- Boninite. The shaded field represents published data from the Arakapas Fault Zone, for comparison (Gass et al., 1994). See text for explanation.

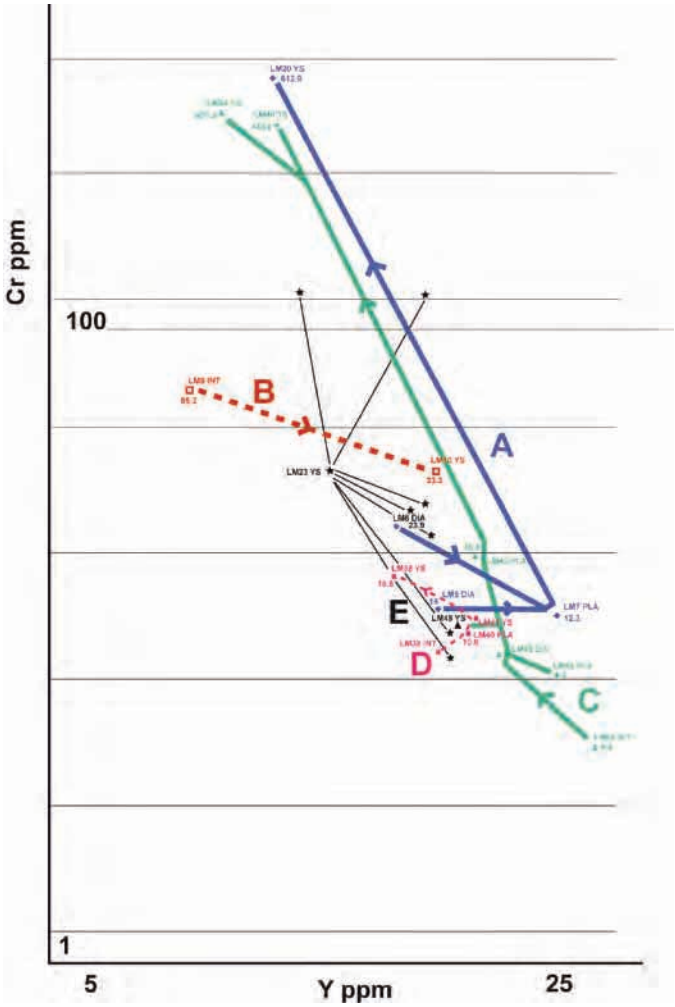

Fig. 14 - Geochemical progression in Cr vs Y in the composition of cross-cutting dykes in selected sections of the Pyrgos road section, north Troodos margin (see A-E in Fig. 6; see also Fig. 2 for the location of the sections. Sections A and C show an overall trend towards a boninitic-type composition (see Fig. 11).

SOUTH-TROODOS SECTION

An exceptionally well exposed ~ N-S road section was studied through the sheeted complex (Fig. 1). Approaching from the south, the section of sheeted dykes extends from Kalo Chorio in the centre of the Arakapas valley, then turns eastwards to Zoopigi, following the road F139. The section terminates in massive gabbro in the north (Fig. 15). The south-Troodos section samples progressive higher levels of the oceanic crust from north to south owing to the ~ E-W orientation of the dykes near the Arakapas Fault Zone.

The objectives of the fieldwork in this section were to characterise the magmatic and structural character of the road section, in a manner similar to the Pyrgos road section in the north. In particular, well-exposed sections of the outcrop along the road were documented for lithology, cross-cutting relationships and the dip and strike of dykes. Given the proximity to the Arakapas Fault Zone, attention was given to the orientation and kinematic relations of faults. Since the section is much shorter than the Pyrgos road section, an attempt was made to document as many of the faults as possible. The outcrop ranges from nearly continuous in the northern and central portions of the section, to discontinuous in the south. Numerous local outcrops were studied (133 in all), in which 256 dykes were described and documented, including width and orientation.

Local lateral variation in the sheeted fabric was assessed by studying outcrops along a dirt road to the east of the road section (halfway along the transect; Fig. 15). Outcrops were also briefly examined to the east and the west of the road section and within the Arakapas Fault Zone, for comparison.

The road section studied is ~ 5 km to the west of a section from which Bonhommet et al. (1988) obtained palaeomagnetic data. The section studied by these authors section allowed palaeomagnetic sampling for tens of kilometres from south to north. The interval of sheeted dykes is shorter in the section studied by us. However, the exposure is better, especially of the critical southerly part near the Arakapas Fault Zone. On a regional scale the two sections are sufficiently close to be interpreted together.

DYKE LITHOLOGIES

Below, the road transect is described, working upwards through the crust (i.e. from north to south). The northern end of the transect is characterised by a kilometre-sized body of spheroidally weathered, massive gabbro, as previously mapped (Gass et al., l991; Fig. 15). The gabbro is made up of altered olivine, plus intergrown clinopyroxene, which is partially replaced by chlorite. Uralite and magnetite are also present. The gabbro is juxtaposed with sheeted dykes to the south by a poorly exposed low-angle fault zone.

The most northerly part (lowest crustal levels) of the sheeted complex is almost entirely made up of grey sheeted diabase dykes (Fig. 15) dipping to the southwest at ~ 20°. Steeply dipping, brown diabase dykes occasionally cut the predominant grey diabase dykes. In addition, dark dykelets (< 20 cm wide) intrude a few pre-existing faults. To the south, the sheeted diabase dykes include screens of quartz-bearing microgabbro (up to 2 m across), of locally variable grain size. The microgabbro is crosscut by grey diabase, which is in turn crosscut by brown diabase dykes. The gabbro is predominantly fine grained but also contains inclusions of coarser material of similar mineralogy. The composition is largely feldspathic with minor quartz crystals, together with minor altered clinopyroxene, chlorite and medium-grained magnetite crystals. The gabbro is cut by numerous veins of hydrothermally derived quartz. Small angular gabbro xenoliths occur within some of the diabase dykes (Fig. 16a).

Further south (~ 1 km south of the gabbro; Fig. 15), the dykes become wider, on average, and relatively more abundant until they make up the bulk of the outcrop. Several dykes are cut by quartz-veined breccia (30 cm-1 m wide) of hydrothermal origin. This veining was followed by faulting.

Further south again (~ 3 km south of the gabbro; Fig. 15), screens of plagiogranite appear in association with faults. Although screens of plagiogranite and gabbro are both present, outcrops in this part of the section are dominated by grey and brown diabase dykes. Both the grey and the brown dykes vary in colour, size and orientation.

Moving southwards (~ 6 km south of the gabbro), the relative abundance of different lithologies varies from outcrop to outcrop (see Fig. 16 a-c). Plagiogranite and gabbro bodies are typically bounded by faults. Plagiogranite is occasionally present as small (< 30 cm), angular inclusions with chilled margins against gabbro. The gabbro is inferred

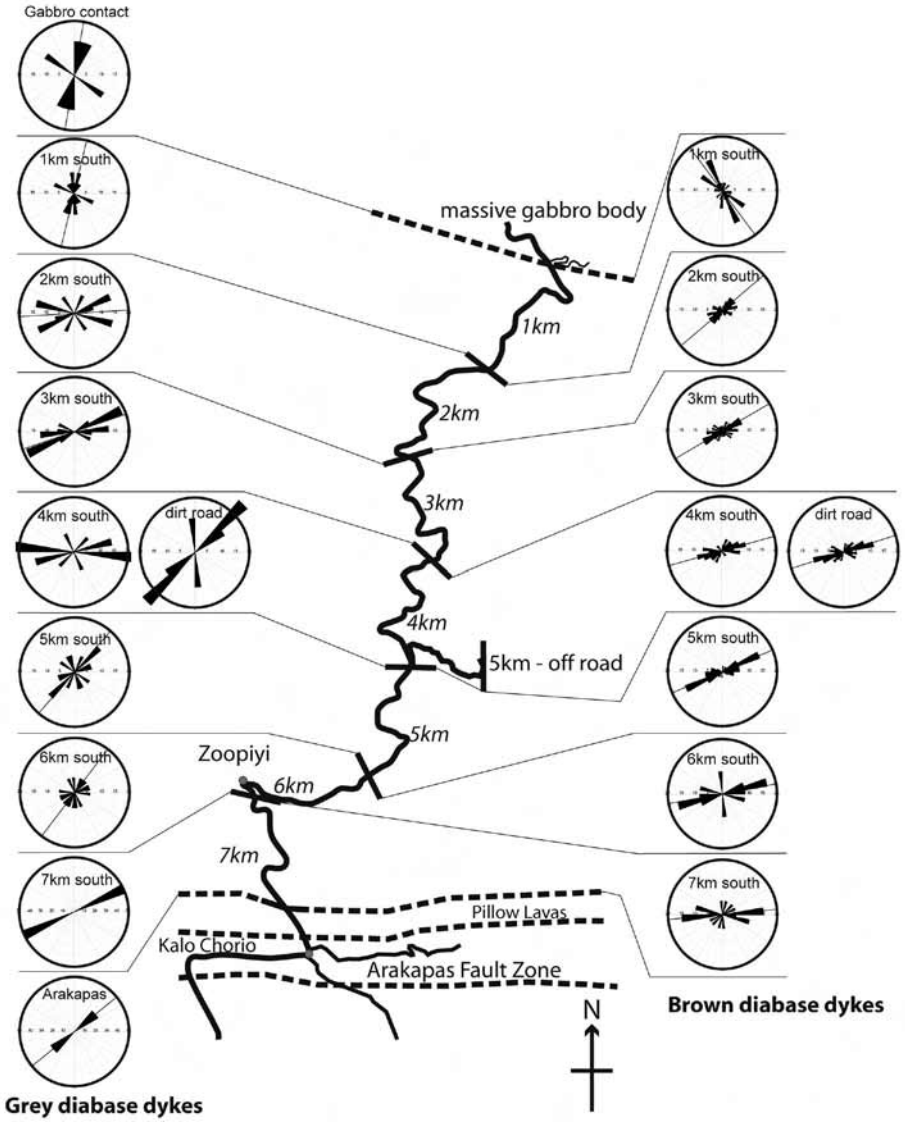

Fig. 15 - Outline map of the road section studied north of the Arakapas Fault Zone, showing rose diagrams of grey and brown sheeted dykes, averaged for 1 km intervals. The late-stage brown dykes show a progressive swing to a more E-W direction towards the Arakapas Fault Zone, whereas the relatively early grey diabase dykes show a more complex pattern (see text for discussion).

to have intruded and dissected a relatively large pre-existing plagiogranite body. Study of the dirt road to the east revealed little lateral variation within the sequence (Fig. 15), suggesting that the road section is representative of a wider area.

The plagiogranites exhibit a groundmass of mostly quartz (50-55%) and plagioclase, plus occasional magnetite. Large phenocrysts of quartz and feldspar are commonly present, together with small quantities of chlorite (commonly located between crystals). Less quartz-rich varieties are classified as tonalities, with quartz (30-35%), plus plagioclase (albite) and also minor amounts of hornblende. Magnetite makes up ~ 5-10% of the rock and is locally associated with chlorite.

Southwards again (> 10 km south of the start of the section; Fig. 15), the lithologies continue to vary in abundance, with the plagiogranite being intruded by gabbro, then by grey diabase dykes and finally by brown diabase dykes (Fig. 16 b-d).

Within 2 km of the Arakapas Fault Zone, plagiogranite disappears, while dark coloured, relatively fine-grained basaltic dykes become common, both as fine-grained aphyric basalt and as coarser-grained plagioclase-phyric basalt. In one place basaltic material is found as angular inclusions (< 60 cm across) within massive gabbro.

The exposure degenerates towards the southern end of the section. The sheeted dykes give way to pillow lavas over < 30 m, although a clear contact is not exposed. The southern end of the road transect is dominated by basaltic pillow lavas that are occasionally intruded by basaltic or boninite-type dykes (0-10% of the outcrop). Further east, towards the town of Arakapas, the fault zone includes pillow basalt, lava breccia, hyaloclastite and isolated dykes (Simmonian and Gass, l978; Gass et al., l994).

Throughout the section, brown diabase dykes generally cut grey diabase dykes (e.g., Fig. 16b, c, d). The grey diabase dykes are similar to those of the Troodos sheeted complex as a whole, as observed in the northern transect (see above). The brown dykes occur either individually or as swarms. The individual brown dykes vary in width from 0.5 to 3 m. Both the grey and the brown dykes show very variable orientations, especially towards the Arakapas Fault Zone. In some sections both the grey and the brown dykes are similarly inclined (Fig. 16c, f), whereas in a few examples, the late-stage brown dykes are inclined at low angles (Fig. 16b, d), suggesting very strong horizontal-axis rotation. In addition, the brown dykes are commonly sinuous and may even bifurcate, deviate, end abruptly or exploit faults or other zones of weakness.

Fig. 16 - Field photographs of lithologies and structures along the road section studied to the north of the Arakapas Fault Zone. a- Small xenoliths of gabbro within grey sheeted diabase dyke; b- Typical grey sheeted dykes that are transected by a late-stage brown dyke at a low angle. Such relations indicate a complex rotation history; c- Classic outcrop (ideal for teaching), which shows early plagiogranite, cut by grey diabase dykes and then by brown diabase dykes. Towards the southern end of the transect (opposite a small blue industrial building); d- Irregular late-stage brown dykes cutting more steeply dipping grey dykes and plagiogranite, indicative of multistage rotation; e- Grey diabase dykes cut by small-scale listric extensional faults, which have been intruded by plagiogranite and re-faulted; f- Complexity of faulting affecting high-angle dykes. Plagiogranite is cut by grey dykes and then by brown dykes, which together are crosscut by planar extensional faults.

To determine if any trends exist, the recorded dips of the grey versus the brown dykes were averaged for different parts of the section, as shown in Fig. 17. In general, the average dips of both the grey and the brown dykes increases towards the Arakapas Fault Zone. In addition, the average dip of the brown dykes is ~ 15° steeper than the grey dykes. The gabbro intrusion is cut by occasional, widely spaced, fine-grained diabase dykes (1-3 m thick), dipping at ~ 60-80°. The gabbro is cut by steeply inclined shear planes and also by small normal faults, with displacements of < 1 m.

One kilometre south of the gabbro body, and within the gabbro body itself, the grey dykes are orientated generally NNE-SSW (Fig. 15). Grey dykes are sparse (< 4 per kilometre) in the northernmost 1 km of the section, south of the gabbro body, and also in the southernmost 2 km of the transect near the Arakapas Fault Zone. A weak NE-SW trend is detectable in the mid part of the section including the dirt road extending eastwards. Beyond 6 km south of the massive gabbro the grey dykes show a more E-W orientation. In contrast, the brown dykes are less variable in orientation (Fig. 15).

The grey dykes are invariably crosscut by brown dykes rather than vice versa (Fig. 18a and c). The local crosscutting relations imply that grey dykes were originally rotated about an assumed horizontal axis and then cut by the brown dykes. Some of these dykes were later rotated in the opposite direction to produce the present geometry (e.g., Fig. 18b), again assuming originally near-vertical intrusion. However, elsewhere both sets of dykes commonly tend to be sub-parallel (Figs. 16c; 18b).

FAULTS

The N-S road section is cut by numerous faults of different scale and orientation (Fig. 16e - f). Fault orientations and crosscutting relations were recorded wherever possible (e.g., see Fig. 18a - c).

Small-scale faulting is ubiquitous throughout the sections studied, with a large variation in fault type, fault orientation and fault displacement. Some 127 faults were recorded within the road section. Of these, 83 show observable kinematic relationships in the form of measureable fault offsets, directional slickensides or imbrication within fault breccia. The most common fault type is normal (extensional) faults of which 30 were recorded. Outcrop-scale, curved (listric) extensional faults were occasionally observed (see Fig. 16c). Some 15 reverse faults were noted. In addition, some 49 strike-slip faults were recorded (Fig. 19), most of which are represented by shear zones that have unclear senses of movement. Ten of the strike-slip faults are represented by left-lateral faults whereas only one right-lateral fault was documented.

The late-stage brown dykes are cut by normal faults, together with a small number of reverse faults and strike-slip faults. However, many faults lack kinematic constraints. Mutual crosscutting relationships are rare such that a relative chronology of fault phases could not be inferred, except very locally. However, the rotation of the grey dykes relative to the brown dykes implies that extensional faulting must have occurred prior to the injection of the brown dykes and in some cases again afterwards to rotate brown dykes to low angles (see Figs. 16b and 18a, c).

The distribution of the different fault types in relation to their distance from the Arakapas Fault Zone is plotted in Fig. 20, although it must be emphasised that the sense of movement on the majority of the faults is unknown. There are few obvious trends in the data from north to south. However, sinistral strike-slip fault zones are more abundant towards the Arakapas Fault Zone, whereas normal faults are relatively more abundant further north towards the massive gabbro. The contact with the gabbro body corresponds to a marked increase in the intensity of shearing which is interpreted as the expression of an extensional (or transtensional) detachment. The data were also plotted on stereonets although this did not reveal meaningful patterns, reflecting the complexity of faulting and the scarcity of fault kinematic data.

GEOCHEMISTRY

Eleven samples of relatively unaltered typical grey diabase dykes and seven of typical brown diabase dykes were chemically analysed (see Tables 3 and 4). In addition, six samples of relatively fine-grained, basaltic dykes were also analysed. One sample of boninitic lava from the Arakapas Fault Zone was also analysed for comparison with the analyses published by Gass et al. (1994). Several samples of plagiogranite, olivine gabbro and quartz gabbro were also analysed (Cooke, 2013) to aid rock type identification.

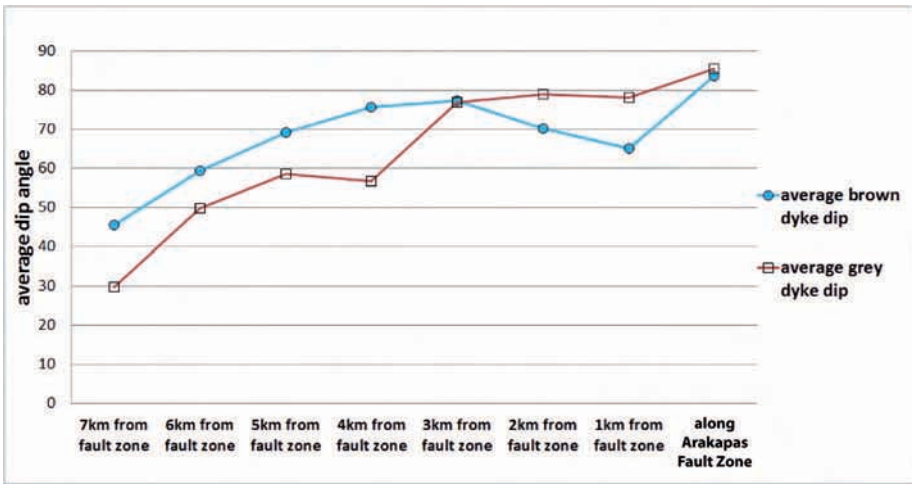

Fig. 17 - Average dip angle of brown and grey diabase dykes in relation to distance from the Arakapas Fault Zone. The late-stage brown dykes are generally more steeply dipping than the early-stage grey dykes, especially towards the fault zone.

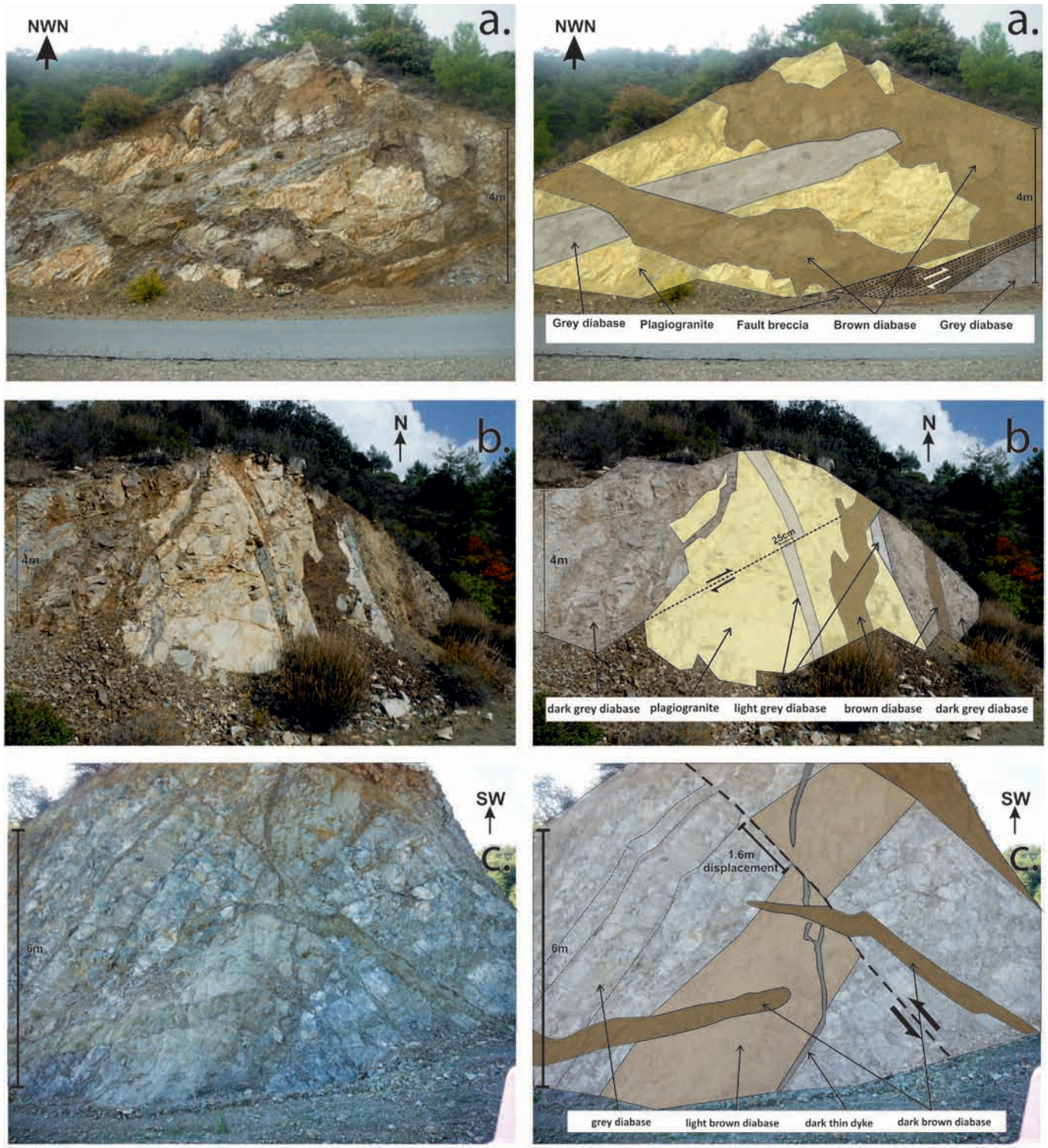

Fig. 18 - Annotated field photographs demonstrating multi-phase intrusive and structural relationships along the south-Troodos road section.
A-A- 4 km south of the gabbro (in the north) showing late-stage, E-W orientated, brown dykes cutting older grey diabase (orientated NE-SW). Both dykes cut plagiogranite; the entire outcrop underwent faulting with the formation of fault breccia.
B-B- Along a dirt track to the east of the section studied, 5 km south of gabbro (in the north). Early plagiogranite is transected by dark grey diabase. The plagiogranite is also cut by light grey diabase, which shows fault displacement (25 cm). The intrusions are orientated ~ E-W.
C-C- 3-4 km south of the gabbro (located in the north). Relatively early-stage grey diabase dykes cut by a light brown low-angle diabase dyke (2 m thick). This was, in turn, cut by a thin black dyke and then reverse faulted (with a throw of 1.6 m). Darker brown dykes then intruded the outcrop at orientations of 163°/65°N and 158°/81°N (strike and dip).

Table 3 - X-ray fluorescence data for lithologies from the south-Troodos transect, north the Arakapas Fault Zone.

	Grey diabase											Brown diabase						
Sample name	AC-01	AC-03	AC-04	AC-07	AC-11	AC-14	AC-18	AC-19	AC-23	AC-26	AC-33	AC-05	AC-13	AC-16	AC-17	AC-21	AC-22	AC-24
Major Elements (wt%)																		
SiO2	55.08	52.71	59.54	54.21	49.96	51.94	53.47	49.65	52.99	51.77	52.27	52.17	53.63	51.12	54.22	52.25	50.59	49.49
Al2O3	14.54	12.78	13.46	15.30	15.49	13.36	14.31	16.24	14.88	17.16	15.70	11.19	15.21	15.68	14.46	15.07	14.93	17.48
Fe2O3	9.02	9.24	14.25	9.23	9.02	9.31	13.13	10.27	13.33	8.95	9.98	9.22	11.12	12.19	13.47	12.97	9.44	7.46
MgO	7.11	10.33	3.85	7.52	7.78	9.31	5.57	6.88	3.90	7.09	6.48	12.46	4.88	5.66	4.52	3.62	7.81	8.49
CaO	5.36	6.57	0.90	4.96	12.12	11.68	4.22	9.59	4.25	11.85	10.10	9.89	5.26	9.17	3.83	5.67	10.86	11.29
Na2O	5.71	4.30	3.65	5.52	1.89	1.56	3.89	2.75	6.31	1.09	1.81	0.38	5.63	2.03	4.74	6.14	2.57	1.82
K2O	0.085	0.028	0.174	0.092	0.098	0.111	0.278	0.357	0.001	0.029	0.087	0.292	0.065	0.057	0.288	0.006	0.172	0.239
TiO2	0.520	0.230	0.690	0.349	0.642	0.329	1.291	0.579	1.411	0.406	0.778	0.213	0.855	1.075	1.299	1.350	0.808	0.307
MnO	0.201	0.160	0.083	0.108	0.148	0.147	0.204	0.178	0.202	0.139	0.178	0.168	0.162	0.205	0.187	0.176	0.191	0.142
P2O5	0.024	0.002	0.037	0.008	0.027	0.007	0.072	0.021	0.094	0.020	0.048	0.001	0.050	0.059	0.080	0.090	0.039	0.002
LOI	2.33	3.32	3.24	2.36	2.77	1.79	3.40	3.09	2.10	1.39	2.20	3.60	2.70	2.55	2.55	2.64	2.29	2.89
Total	99.98	99.68	99.87	99.66	99.96	99.53	99.84	99.61	99.47	99.89	99.63	99.58	99.56	99.79	99.64	100.00	99.70	99.60
Sample name	AC-01	AC-03	AC-04	AC-07	AC-11	AC-14	AC-18	AC-19	AC-23	AC-26	AC-33	AC-05	AC-13	AC-16	AC-17	AC-21	AC-22	AC-24
Trace elements (ppm)																		
Sr	80.8	26.7	45.8	90.9	192	86.9	78.3	170	166.7	71.8	87.9	113.4	57.3	80	88.4	20.7	41.8	18.8
K	705.621116	228.621245	1442.12355	766.76112	814.901084	923.99011	2307.79615	2963.60873	8.301425	240.741325	722.223975	2427.79325	539.592625	474.84151	2390.8104	50.5556783	1427.8451	1983.37646
Rb	0.5	0.4	1	0.6	0.6	0.8	1.4	2.1	1.2	0.4	0.5	4.6	0.5	0.1	1.4	0.7	0.1	0.2
Ba	6.9	2.5	0.8	4.4	15.3	12.3	3.2	23.8	23	9.6	14	35	3	2.7	11.3	0.1	1.6	
Nb	1	2.8	6.3	1.8	0.3	1.2	0.8	1.2	0.8	0.9	0.9	2.2	0.8	1	1.1	1.3	0.9	1.3
Ce	2.5	3.1	6.1	2.9	3.1	2.6	6.5	1.6	5.2	2.6	4.2	0.7	5.7	6.1	7.5	8.5	1	7.4
P	104.738736	8.90279256	163.08694	35.4366057	119.245051	30.090566	314.216208	91.646394	410.226716	87.28228	209.477472	4.38593457	218.2057	258.704678	349.12912	394.232238	170.200446	7.89904634
Zr	20.8	9.9	24.3	10.5	22.8	9.5	50.7	15.4	37.9	17.9	39.7	7.8	38.4	26.7	60.7	68.7	6.5	71.1
Ti	3117.4	1375.8525	4135.53085	2093.2142	3846.43996	1972.29505	7739.545	3471.105	8458.945	2433.97	4664.11	1277.2947	5125.725	6446.7832	7787.505	8092.95025	4843.96	1839.23603
Y	13.7	7.7	17.5	11.3	14.3	9.4	26.6	14	19.2	13.1	21	7.2	22.1	18.5	30.9	33	10.2	35.1
Zn	61.9	64.4	41.3	72.6	56.8	39.8	187.2	74	54.8	58.5	82.9	72.1	93.4	80.2	158.3	105.4	77	122.1
Cu	53.5	122.1	1725.9	119.2	16	11.3	7	41.4	96.6	63.7	81.8	91.4	100	8.2	22.4	16.4	168.1	43.2
Ni	57.8	179.7	11.7	55.3	70.7	90.7	13.1	39.5	85.5	45	28.8	244.6	28.4	34.9	17.5	17.1	46.8	17.6
Cr	175.6	610		40.8	270.5	458.5		51.3	319.8	133.3	24.5	868.4	11.7	32.2		4.4	85.5	1.7
V	290.3	255.5	439	283.5	295.5	252.5	508.6	312.4	266.9	261.2	277.4	237.4	338.8	308.6	474.1	417.7	277.4	441.8
Sc	40.7	43.7	49.1	40.4	50.6	50.5	46.3	46.8	49	47.3	40.1	41.9	39.7	45	44.6	36.5	49.5	40.6
La																		
Nd	2.9		1.7	1.1	1.4	0.9	5	2	5.8	1.6	4.2	0.6	5	2.7	6.4	7.9	0.7	8.1
U		0	0.1	0			0.1	0.1	0		0.1				0.2	0.3		0
Th	0.1	1	0.2	0.3	0.2					0.4	0.2	1.1	1.1	0.8			0.4	
Pb	0.5	1	1.1	1	1.3	0.8	0.8	0.9	0.8	1	0.1	1.1	0.9	0.7	0.7	0.8	0.7	0.8

Major elements in wt.% oxide; trace elements in parts per million (ppm). Blank entries = below detection.

Table 4 - X-ray fluorescence data for additional lithologies from the south-Troodos transect, north the Arakapas Fault Zone.

	boninite	pillow basalt			basaltic dykes			plagiogranite		olivine gabbro				quartz gabbro	
Sample name	AC-02	AC-06	AC-08	AC-28	AC-15	AC-29	AC-30	AC-12	AC-20	AC-09	AC-10	AC-25	AC-27	AC-31	AC-32
Major Elements (wt%)															
SiO2	52.55	54.47	51.73	53.83	52.39	76.52	54.78	73.74	76.50	50.50	49.67	53.30	51.64	74.31	73.62
Al2O3	12.16	15.29	16.36	15.51	14.14	11.56	14.04	13.17	12.06	16.26	15.69	16.14	13.77	12.74	13.85
Fe2O3	7.53	10.21	11.55	9.70	10.04	3.58	10.64	3.76	2.95	10.21	10.04	9.27	8.70	2.51	2.60
MgO	14.19	6.45	3.70	6.68	5.40	0.36	7.11	0.27	0.31	7.10	7.00	7.00	8.96	0.09	0.73
CaO	10.58	4.08	7.37	4.51	6.12	1.83	4.98	3.13	1.94	10.83	10.97	10.96	10.83	4.92	2.87
Na2O	0.50	5.86	5.31	5.73	4.79	4.40	5.12	4.30	4.30	1.43	2.34	1.27	0.31	4.26	3.86
K2O	0.073	0.033	0.006	0.002	0.037	0.297	0.094	0.161	0.278	0.079	0.056	0.009	0.168	0.006	0.440
TiO2	0.187	0.414	0.707	0.298	0.651	0.276	0.662	0.282	0.172	0.855	0.953	0.434	0.297	0.282	0.462
MnO	0.131	0.084	0.228	0.125	0.165	0.021	0.154	0.032	0.016	0.214	0.191	0.168	0.159	0.019	0.025
P2O5	0.000	0.011	0.036	0.004	0.032	0.056	0.033	0.060	0.017	0.025	0.064	0.018	0.005	0.051	0.077
LOI	1.67	2.95	3.09	3.16	5.97	0.74	1.93	0.79	0.62	2.50	2.50	1.12	4.58	0.66	1.20
Total	99.56	99.86	100.09	99.55	99.73	99.64	99.55	99.69	99.16	100.01	99.47	99.71	99.42	99.86	99.74
Sample name	AC-02	AC-06	AC-08	AC-28	AC-15	AC-29	AC-30	AC-12	AC-20	AC-09	AC-10	AC-25	AC-27	AC-31	AC-32
Trace elements (ppm)															
Sr	27.7	49.2	24.4	63.2	28.1	138.3	116.1	123.8	122.6	118.6	153.9	135.8	89.5	140.2	167.2
K	609.656652	274.445111	51.0537638	16.60285	304.413255	2465.02514	776.43228	1333.87297	2307.79615	653.986262	464.8798	74.3392609	1394.6394	50.0575928	3654.20427
Rb	0.8	0.3	0.2	4	0.4	2	0.4	0.7	1.1	0.7	0.5	1	0.3	0	3
Ba	15.4	4	0.4	15.6		19.8	18.2	65.9	18.1	14.3	6.5	5.7		4.9	25
Nb	0.8	3.8	1.7	2.1	0.8	1.8	0.7	1.7	2.1	1.7	0.6	0.4	0.9	1.9	2.1
Ce		4.5	4.1	0.6	7.8	16.1	3.8	15	14.2	5.4	6.4	2.5	3.4	18.5	11.1
P	0	49.7508996	156.56259	17.456456	138.97521	242.426533	143.295683	260.71217	74.189938	110.193879	279.303296	78.1612817	21.82057	223.682663	337.716962
Zr	7.1	14.7	26.3	7.7	48.4	90.2	16.2	63.8	75.1	30.2	47.8	9.3	18.4	91.7	145.6
Ti	1119.0267	2480.8509	4239.96375	1786.51	3904.99313	1653.00135	3966.74163	1691.9089	1031.14	5128.54265	5713.235	2600.7509	1780.515	1693.01798	2771.4885
Y	7.5	14.8	19.4	11.2	25	36.4	13	48.1	50.8	21.4	25.1	7.6	13.1	43.3	41.3
Zn	52.9	83	95.6	76	90		40.6	14		62.2	40.4	34.3	41.6		8.7
Cu	75.2	121.3	48.6	86	286.7	5.3	5.8	7	15.8	9.8	242	8.2	17.4	2.6	3.9
Ni	293.7	46.2	22.3	213.7	36.7	2	70.8	0.5	0.1	47.8	75.1	57.3	58.3		2.8
Cr	1175.3	10.6	2	597	110.4	3.9	219.7	4.2	3.8	105.4	203.4	63.3	47.2	4.1	6.3
V	187	332	407.6	257.7	392.4	14.3	326.1	10.2	6.9	321.7	289.8	232.5	216.9	3.6	24.2
Sc	40.8	42.9	44.1	42.5	46.3	16.1	50.7	17.4	15.5	46.9	44.5	53.1	48.8	17.3	10.4
La		0.2		1.6		5.9		4.7	2.9					2.7	2.6
Nd	0	1.2	4.1	0.6	4.5	10.3	1.4	13.5	10	3.4	5.7	0.2	2.8	10.4	10.2
U	0	0	0.2		0.2	0.3		0.4	0.1		0.3	0		0.4	0.5
Th	0.6	0.6	0.3	0.8		1.2	0.7	0.9	0.7			0.1	0.9	1	0.7
Pb	0.9	2	1.7	1.4	0.1	0.6	0.8	0.6	0.1	0.5	0.7	0.8	0.2	0.1	0.3

Major elements in wt.% oxide; trace elements in parts per million (ppm). Blank entries = below detection limit.

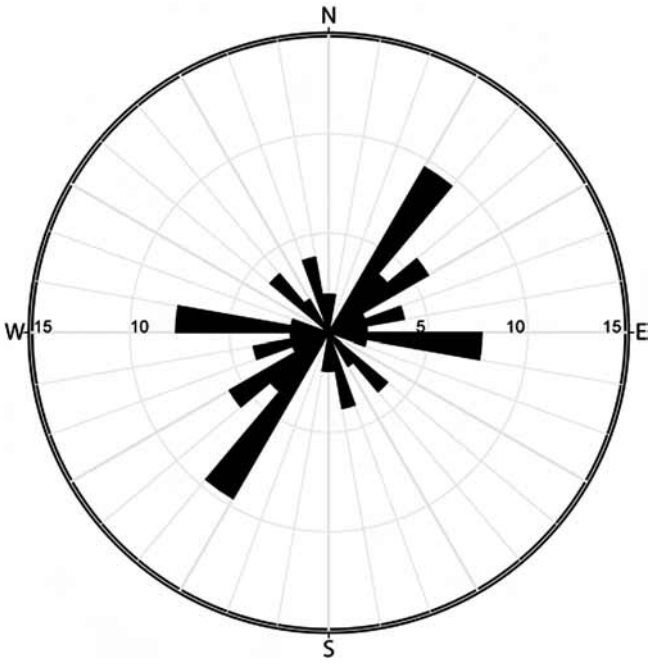

Fig. 19 - Rose diagram of the orientations of strike-slip faults, as measured along the road section to the north of the Arakapas Fault Zone (10° class intervals; number of measurements indicated by radius); see text for explanation.

The specific aims of the analyses were as follows: 1. To test for any systematic chemical changes from north to south in the section; i.e generally upwards through the crust; 2. To test for any systematic chemical variation within individual, locally intact sections; 3. To determine if any of the dykes could be feeders for the well-documented boninitic lavas exposed within the Arakapas Fault Zone; 4. To compare the northern and southern Troodos margin data sets to determine if any significant differences exist, specifically related to proximity to the transform fault zone.

Within the dykes generally, the crystals are slightly aligned, resulting in a sub-trachytic texture. The grey diabase dykes locally contain olivine, together with plagioclase, clinopyroxene and rarely orthopyroxene. Olivine is commonly pseudomorphed by chlorite. Chloritisation is prevalent as fibrous chlorite and peninite (blue chlorite). Uralite is also present, plus secondary epidote, green fibrous actinolite and opaque magnetite. The later stage brown diabase dykes are predominantly plagioclase and clinopyroxene-phyric. Augite is largely replaced by uralite. Radiating chlorite crystals are present, rarely together with epidote and common opaque minerals (e.g., magnetite). Plagioclase is typically altered to a mottled texture. The grey diabase dykes appear to contain a higher abundance of chlorite compared to the brown diabase, which may reflect greater degrees of hydrothermal alteration (see Staudigal et al., 1986). As in the northern section, brown-weathering dykes contain a relatively high abundance of opaque iron-rich minerals compared to the grey dykes, which may again explain their red colour, where oxidised.

For ease of comparison the data were plotted on the same types of diagrams as the north-margin transect. On the rock classification diagram, the lithologies plot in the Tholeiitic basalt field (Fig. 7b), although two samples plot in the Andesite/Basalt field. The rock compositions are more scattered than for the north-margin diabase (Fig. 7a). The Ti values in the south-margin lithologies mostly lie in the same range as the north-margin data set, although several of the grey and and brown dykes are relatively enriched in Ti and Zr (see Tables 3 and 4).

The MORB-normalised spider plots (Fig. 8c - f) show that that the compositions of the grey dykes and the brown dykes, although variable, lie within a similar range, suggesting that they were fed from chemically similar magmas. On the Ti vs Zr diagram (Fig. 9) the grey diabase dykes plot quite coherently, whereas the later-stage brown dykes are scattered. The grey dykes are compositionally similar to the small number of basaltic extrusives analysed from the southern end of the section, within the Arakapas Fault Zone. On the Zr/Y vs Zr diagram (Fig. 10b) and also on the Cr vs Y diagram (Fig. 11b), the grey and brown dykes show no clear differences overall. For comparison, previously analysed dykes from the Arakapas Fault Zone (Gass et al., 1994) are marked as a shaded field in Fig. 10b. Some examples of both the grey and the brown dykes plot in the boninite field.

The dykes and basalts show a marked subduction influence on the geochemical diagrams (e.g., negative Nb anomalies in Fig. 8c - f). This is further highlighted on the V-Ti diagram on which the south-margin samples straddle the IAT and the MORB + BAB field, with around half of the

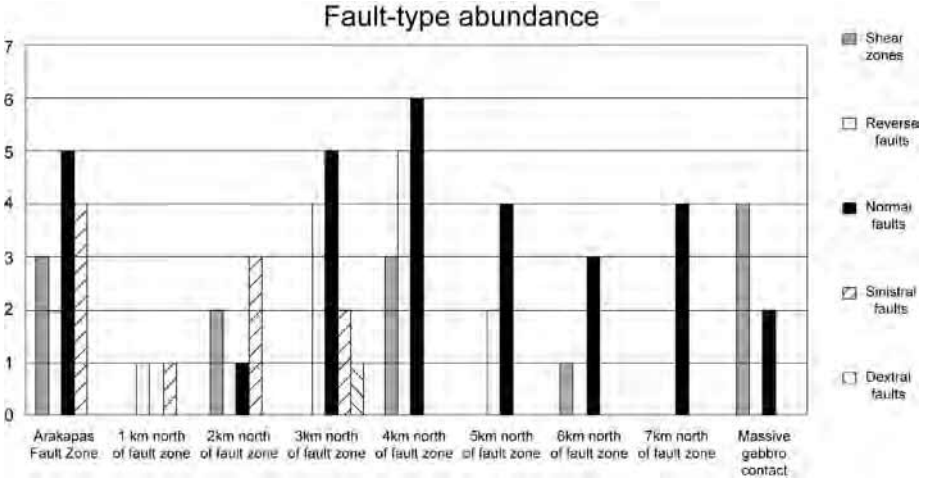

Fig. 20 - Abundances of the different fault types in relation to distance from the Arakapas Fault Zone. Left-lateral (sinistral) faults are most abundant towards the fault zone, while right-lateral (dextral) faults are very rare. (Note: no faults were recorded ~ 1 km from the fault zone as a result of limited exposure along the road section).

samples plotting outside the recognised fields. On the TiO_2 vs MnOx10 vs P_2O_5 diagram both the grey and brown dykes plot in the boninite or the island arc field (Fig. 13).

When the north and south Troodos data sets are taken together and compared, several points emerge: on the the Ti vs Zr diagram (Fig. 9) the north-margin dykes are slightly enriched in Ti relative to Zr compared to the south-margin section. On the Zr/Y vs Zr diagram (Fig. 10) the north Troodos margin dykes are slightly enriched in Zr compared to the extrusives of the south-Troodos section. On the Cr-Y diagram (Fig. 11a - b) the two data sets are similar. However, the north-Troodos relatively low-angle dykes (mostly grey diabase) tend to be relatively depleted in Cr vs Y compared to the grey diabase dykes from the south-Troodos data set. A greater proportion of the south-Troodos samples are highly depleted and plot in the boninite field compared to the north-Troodos data set.

DISCUSSION

Below, we discuss the implications of the northern transect for spreading processes and the implications of the southern transect for both spreading and transform processes.

Spreading processes

The present study demonstrates the role of extension in relation to the lithology and the geochemistry of the different types of intrusion. In the eastern segment of the north-Troodos section, where the dykes are on average steeply dipping, extension and magma supply are inferred to have been approximately in balance during the construction of this part of the sheeted complex. In the western segment where the dykes are on average less steeply inclined, in these areas extension in assumed to have exceeded magma supply, at least locally, favouring horizontal-axis dyke rotation. In the west, the major east-dipping, low-angle shear zone, which is correlated with the eastern margin of the Solea Graben, implies an episode of intense extension. This extension appears to have post-dated magmatism at least locally because the shear zone as a whole is not cut by dykes.

The data collected on the sheeted complex in the two areas are relevant to the evaluation of several alternative tectonic-magmatic models of sea-floor spreading in the Troodos ophiolite.

Steady state spreading from a single spreading axis

In this interpretation, sea-floor spreading proceeds by regular dyke intrusion at a very narrow spreading axis (< 10s of metres), with the dykes rotating as they cool and subside away from the spreading axis. Preferential one-way chilling directions, as reported from the sheeted dykes, assumed this type of 'infinite onion' spreading model (Kidd and Cann, 1974). High-temperature hydrothermal alteration occurs near the spreading axis in this interpretation, while major normal faulting to form half-grabens takes place at the ridge flanks (Cann and Gillis, 2004). Consistent with this model, in the north Troodos (Pyrgos) road section, mineralised diabase screens are cut by later less mineralised or unmineralised dykes. There is, therefore, no support in this particular section for the concept that high-temperature hydrothermal alteration and massive sulphide genesis was driven by late-stage, off-axis intrusion (Varga and Moores, 1990; Bettison-Varga et al., 1992; Varga et al., 1999).

The most obvious debateable point concerning the first model, above (steady-state spreading) is that the sheeted dykes are disposed in several large-scale, variably dipping fault blocks which have been interpreted as discrete tectonic grabens (e.g., Varga and Moores, 1985; 1990). A more consistent dip in the same direction (eastwards) would be expected if regular spreading had taken place from a single spreading axis located to the west of the present outcrop. Also seemingly inconsistent with the first model are the patterns of intrusion of gabbro and plagiogranite, which were both preceded and succeeded by voluminous sheeted diabase intrusion in different exposures. Such relationships are explicable utilising the concept of multiple small magma chambers, as inferred by the mapping of the plutonic core of the Troodos Massif (Malpas, 1990).

Multi-stage spreading related to switching spreading axes

Mapping of a large part of the northern Troodos area has revealed that the sheeted dykes dip inward to form morphological grabens in several areas (Fig. 1). Spreading initially created an axial graben, as represented by the Solea Graben that was later abandoned, with the formation of a new spreading axis up to several tens of kilometres away (Varga and Moores, 1985; 1990). Spreading was inferred to have jumped episodically eastwards, mainly based on the eastward dip of sheeted dykes exposed between the Solea and Mitsero (~ Epiphanios) Grabens. Based on structural study, the Solea Graben was interpreted to have formed during seafloor spreading or shortly afterwards (Hurst, 1994).

Spreading from a single spreading axis, punctuated by structural-magmatic discordances

In this model, morphological grabens were created by the interplay of magmatism and extension at a single spreading axis (Allerton and Vine, 1987). High magma supply resulted in structurally coherent, steeply dipping spreading fabrics, whereas relatively low magma supply triggered extensional faulting and the development of regionally extensive detachment faults, which were inferred to have been located near the base of the sheeted dyke complex. The Solea Graben was noted to be an asymmetrical feature, extending ~ 10 km to the west of the graben axis but only 3-4 km to the east of this structure. The western boundary of the graben was reported to abut a relatively simple area of nearly vertical dykes, although this statement now needs to be qualified in view of the additional information provided here for the Pyrgos road section within the Stavros Graben. In the east, the graben was bounded by strongly faulted, generally eastward-dipping dykes reflecting the development of a structural detachment between sheeted dykes and underlying gabbros. This detachment was modelled as being regionally extensive and overlain by variably tilted fault blocks within the northern Troodos area (Allerton and Vine, 1987). The Solea Graben was interpreted as part of the larger-scale western flank of an intermediate-rate to fast spreading ridge.

There are several debateable aspects of above model. First, there is a need to infer an important role for antithetic faulting (i.e. fault blocks that are forward-rotated rather than back-rotated relative to the spreading axis). In this interpretation the spreading axis is assumed to have migrated eastwards with time, which requires the relatively short section of east-dipping dykes of the Solea Graben (compared to the west-dipping dykes) to have resulted from antithetic faulting. The dyke orientations in the vicinity of the Mitsero (~ Epiphanios) Graben imply a more complex geometry

than a simple graben, which could be consistent with off-axis extension and magmatism (Van Everdingen and Cawood, 1985). Major extensional detachment faults separate the sheeted dykes from massive gabbro in some areas (e.g., Lemithou; western Troodos) but not in others (e.g., Mitsero and Mathiati areas; northern Troodos). In the core of the Troodos Massif, mantle rocks are faulted against gabbro along the Amiandos Fault, which is interpreted as a deep-level detachment that developed near the intersection of the southward extension of the Solea Graben with the Arakapas transform fault zone (Nuriel et al., 2009). The evidence, therefore, suggests that a single through-going extensional detachment is unlikely to be present throughout the Troodos.

Allerton and Vine (1991) subsequently adopted an intermediate position between the single spreading axis model and the multi-spreading axis model. They envisaged that spreading originated in the vicinity of the present Solea Graben, whereas the Mitsero Graben was created by off-axis magmatism and tectonic extension to the east of the ridge axis. This was followed by eastward relocation of the spreading ridge to the Larnaca Graben (less well exposed), while generally amagmatic extension continued within the Solea Graben to create its present asymmetrical morphology. This interpretation further suggests that relatively late-stage amagmatic extension may have been important in the Troodos ophiolite generally (see also Gee et al., 1993).

The direction of spreading has also been debated. The spreading axis was assumed to lie to the west of the Troodos by Kidd and Cann (1974) based on their statistically determined direction of preferential one-way chilling. The method was found difficult or impossible to apply to the north Troodos margin section studied because of common hydrothermal alteration of dyke margins or complex intrusion history where relatively low-angle dykes are present.

Several lines of evidence are seemingly inconsistent with a simple one-way chilling process. Interpretation of seismic refraction data from the northern Troodos Massif (Maguire et al., 2000) has revealed a series of large-scale, down-to-the-west normal faults that could be correlated with two major down-to the-west extensional fault zones with the north-Troodos outcrop (e.g., Kakopetria Fault of Hurst et al., 1994). Troodos lavas are inferred to thicken into these faults suggesting a contemporaneous origin related to sea-floor spreading. However, this simple pattern of steep faulting is inconsistent with the variably orientated, commonly inclined to low-angle faults that are mapped in the field (e.g., Allerton and Vine 1991, and references therein). Important ~ N-S faults are known to cut the sedimentary cover (e.g., Kinnaird and Robertson, 2013). Some of these faults could correspond to the structures inferred based on seismic refraction data (Maguire et al., 2006) rather than reflecting original sea-floor spreading structures. The seismic refraction data are, therefore, not a problem for the preferential one-way chilling model (Kidd and Cann, 1974).

It has also been suggested that the sedimentary cover deepened eastwards across the Troodos ophiolite, based on the time when the Troodos extrusives were first covered by Cenozoic pelagic sediments (Cann and Gillis, 2004). This relationship, if valid, would be consistent with the spreading axis being located to the west of the Troodos outcrop, as in the preferential one-way chilling model (Kidd and Cann, 1974). However, the depositional relationships of the base of the Cenozoic cover sequence may not support this interpretation. The sedimentary evidence shows that the northern margin of the Troodos existed as a relative bathymetric high during the Campanian-Maastrichtian, while a bathymetric low existed along its northwestern margin, which was infilled with up to 750 m of volcanogenic sediments, represented by the Kannaviou Formation (Robertson, 1977b; Gilbert and Robertson, 2013). The southern margin of the Troodos was also a relatively low area of seafloor allowing thick hemipelagic and volcanogenic clays to accumulate during the same time period (Moni Clay; see Robertson, 1977c). Considerable tectonic re-organisation of the bathymetry of the Troodos oceanic crust is likely to have accompanied the emplacement of the Mesozoic Mamonia Complex in western Cyprus and the Moni Mélange in southern Cyprus prior to the onset of regional pelagic carbonate deposition during the Maastrichtian (see Robertson, 1977a; 1977b; 1977c; 1990).

Ridge relocation, as in the model of Allerton and Vine (1991), requires any new spreading centre to have transected already crystallised segments of sheeted dykes. This, in turn, implies large-scale intrusion of pre-existing crust, which should be associated with high-temperature hydrothermal alteration. However, such hydrothermal effects were not observed at the boundary between the Solea and Stavros Grabens during this study. The field evidence instead suggests that the boundary between these two grabens experienced strong relatively late-stage amagmatic extension.

In summary, the evidence for the relative location of the spreading axis remains inconclusive based on evidence from the sheeted dykes. However, the field evidence is supportive of episodic relocation of the spreading axis towards the east in present co-ordinates, coupled with (or followed by) a strong component of amagmatic extension. Spreading of the Troodos above a subduction zone (e.g., Pearce and Robinson, 2010) requires the locus of spreading to have migrated towards the subduction zone, as consequence of rollback of the subducting slab. Slab rollback could have resulted in instabilities in spreading and also in amagmatic extension.

MAGMATISM ASSOCIATED WITH THE ARAKAPAS TRANSFORM FAULT ZONE

The relatively large plagiogranite bodies in the southern part of the south-Troodos section intruded at a relatively early stage, in contrast to the north-Troodos transect in which plagiogranites were intruded at a mid to late stage (see above). In the section studied, the plagiogranite outcrops decrease in relative abundance and then disappear northwards, away from the Arakapas Fault Zone. The original dimensions of the plagiogranite intrusions are impossible to specify because they are fragmented by later dyke intrusion; however, the likely scale was tens, to hundreds of metres across. Plagiogranites also cut sheeted dykes within the Arakapas Fault Zone, as exposed south of Arakapas (Gass et al., 1994). Small gabbroic bodies were also intruded into the sheeted dykes within the section studied at a relatively early stage. The occurrence of the plagiogranites could reflect the ease of intrusion of highly fractionated magmas into severely fractured crust within (and near) the transform fault zone.

The late-stage brown dykes are much thicker and more numerous than the comparable brown dykes in the northern transect. Both the grey sheeted dykes and the late-stage brown dykes were fed by magma of similar composition based on the geochemical data. Boninite-type dykes occur only locally in the southern transect near the Arakapas Fault Zone, in which boninite-type dykes and boninite-type extrusives occur extensively. The boninite-type lavas are considered to have

erupted at a relatively late stage after complex deformation of the underlying crust (Gass et al., 1994). The related magmas are inferred to have been created by high degrees of partial melting of previously depleted mantle in a water-rich setting above a subduction zone (Cameron, 1985; Murton, 1989; Gass et al., 1994).

The late-stage dykes, represented by the commonly brown-weathering, isolated dykes have undergone clockwise rotations (about a vertical axis), which on average increase southwards, until the dykes run parallel to the Arakapas Fault Zone in the south. The structural evidence further indicates a complex history in which relatively early grey dykes near the Arakapas Fault Zone experienced initial rotation (about an assumed horizontal axis). The brown dykes were then injected, presumably vertically. This was followed by rotation of both sets of dyke in the opposite direction of the previous tilting (again about an assumed horizontal axis). This differential tilting is not evident further north away from the Arakapas Fault Zone and is thus likely to relate to movements along the transform fault zone.

SENSE OF MOVEMENT ALONG THE ARAKAPAS TRANSFORM

The sense of movement along the Arakapas Fault Zone continues to be debated, utlising three main alternative models, as follows:

1. ***Left-lateral slip between right-offset spreading axes (Fig. 21a)***

The swing in dyke direction towards the transform is explained by intrusion in a transtensional setting (sigmoidal stress regime) in which the dykes were orginally intruded in a progressively E-W direction approaching the transform (i.e. the 'leaky transform' model of Simonian and Gass, 1978). This is consistent with the evidence of intrusion in an extensional or transtensional setting, as noted above. On the other hand, the palaeomagnetic evidence shows that the dykes in the nearby section were rotated clockwise after they crystallised (Bonhommet et al., 1988). Sheeted dykes in the eastern Troodos (Lefkara area) have also undergone clockwise rotations about steeply inclined axes (Allerton, 1988; Allerton and Vine, 1990). In addition, a study of sheeted dykes which form tectonically bounded bodies within the Arakapas Fault Zone has shown that some of these have been significantly rotated in a clockwise direction (Morris et al., 1990; MacLeod et al., 1990). Similar clockwise rotations have also been recorded within the inferred extension of the Arakapas Fault Zone into western Cyprus (Morris et al., 1998). These results show that clockwise rotation affected a much longer segment of the palaeo-transform fault zone than only the Arakapas Fault Zone exposed in southern Cyprus. In addition, more recent palaeomagnetic studies have identified clockwise rotations throughout large areas of the Troodos Massif (Abelson et al., 2002; Granot et al., 2006; Borradaile and Gauthier, 2006; Scott et al., 2012).

2. ***Right-lateral slip at a left-offset spreading axis (Fig. 21b)***

The palaeomagnetically determined clockwise rotations, as summarized above, are interpreted to be a response to simple shear (i.e. frictional coupling) between the Troodos plate and the inferred oceanic plate to the south (in present co-ordinates). The rotations are inferred to have taken place during transform faulting (Morris et al., 1990). The clockwise rotations originated at, or near, the ridge-transform intersection within hot, thin crust. One apparent problem is that the propagation of simple-shear stress from the transform to the spreading axis might be expected to have impeded dyke intrusion. However, the limited structural evidence from the section studied is suggestive of an extensional, or transtensional setting, which would have facilitated dyke intrusion.

Alternatively dyke rotation might theoretically have taken place only after intrusion had ended, in response to a change from pure strike slip to transpression. This could have involved transpression within the transform and/or along a fracture zone outwith the offset spreading axes. Such a corresponding change in stress regime could conceivably have been associated with the well-documented anticlockwise palaeorotation of the Troodos ophiolite (Clube and Robertson, 1986; MacLeod, 1990; Murton, 1990). On the other hand, the latest Cretaceous pelagic sedimentary cover of the Arakapas Fault Zone, as represented by the Santonian to Campanian-aged Perapedhi Formation, shows no evidence of contemporaneous compressional (or transpressional) deformation in the vicinity of the Arakapas Fault Zone (Gass et al., 1994; Robertson, 1997b). The clockwise block rotations are instead likely to have originated at an early stage, close to the ridge-transform intersection.

An apparent problem with the dextral strike-slip model (Fig. 21b) is that a number of oceanic transforms and related fracture zones, including the Clipperton, Pitman, MARK, Atlantis and Kane fracture zones include some segments in which the inferred spreading fabric is suggestive of anticlockwise rotation at a right-slipping transform and vice versa (e.g., Gallo et al., 1986; Macdonald et al., 1986; Livermore et al., 1991; Karson and Lawrence, 1997 a; 1997b; Blackman et al., 1998; Sonder and Pockalny, 1999; Smith, 2013). In these settings, the spreading fabric is generally seen as being defined by the regional-scale trends of abyssal hills or fault lineaments, as identified using swath bathymetry. The deflections of these fabrics towards transform faults can be considered to be broadly comparable to the swing in dyke trend towards the Arakapas Fault Zone. Such swings in ocean floor fabrics have been explained by extension (transtension) within the active transform offset or by late-stage transpression, either within or outwith the active transform offset zone (e.g., Livermore et al. 1991; Sonder and Pockalny, 1999). A transpressional model for the seafloor fabric swing would, however, require a change in the slip direction relative to the active transform that is not documented.

3. ***Left-lateral slip at a right-offset spreading axis (Fig. 21c)***

Cann et al. (2001) propose a mechanism that achieves clockwise dyke rotation at a left-slipping transform. Multiple clockwise rotations are envisaged as taking place within an inside corner strip at the locus of a change from extension to strike-slip (Fig. 21c). This is viewed as being comparable with listric faults being rotated through 90°, with the footwall representing the transform. The authors see this process as being analogous to removing sets of books from a bookshelf one after the other, while the remaining books slip round to progressively lower angles. They cite an example of comparable geometry from the northern segment of the left-slipping Dead Sea Transform, where clockwise solid-block rotations occur along transtensional fault plays (Ron and Eyal, 1985). Assuming that the Dead Sea example is correctly interpreted, this mechanism is, however, unlikely to be generally applicable to intra-oceanic transform faults. In contrast, simple ball-bearing-type rotations are documented in several areas of hy-

phen deformation, including the Eastern Transform Ranges of the San Andreas Fault system (e.g., Nicholson et al., l986a; 1986b). The intra-continental setting of the mechanism proposed by Ron and Eyal (l985) may not be applicable to oceanic ridge-transform intersections, for example the MARK area (e.g., Karson and Lawrence 1997a; 1997b), or the Atlantis Transform (Cann et al., l997; Blackman et al., 1998). In such oceanic areas extensional exhumation to form large-scale detachments ('megamullions') appears to take place along kilometre-scale low-angle, corrugated, detachment surfaces rather than along localized extensional fault splays, as in the intracontinental setting proposed by Ron and Eyal (l985). The corrugations appear to be linear in the oceanic settings, rather than curved, and there are few signs that small-scale blocks rotate as exhumation takes place, as inferred for the intracontinental setting discussed by Ron and Eyal (l985). In consequence, direct comparisons between the observed swings in crustal fabrics near modern oceanic transform faults and the dyke swing towards the Arakapas transform may well be unrealistic.

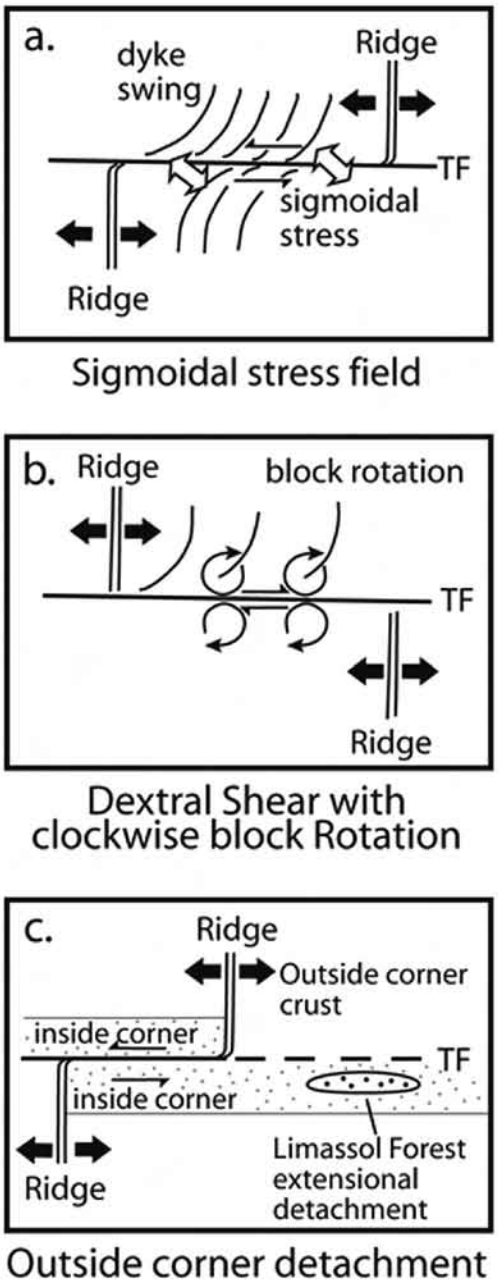

Fig. 21 - Alternative tectonic models for the South Troodos Transform Fault Zone. a- 'Leaky transform' model implying left-lateral slip along the transform; b- Simple shear (frictional rotation) model implying right-lateral slip along the transform; c- Formation in the inside corner strip detachment of a ridge-transform offset zone, implying left-lateral slip. See text for literature sources and explanation.

The limited structural evidence studied from the section north of the Arakapas transform (i.e. sinistral strike-slip faulting), at first sight is seemingly incompatible with model 2 (right-lateral slip along the transform), but more consistent with models 1 and 3. However, in the right-lateral slip model (model 2), the sinistral faults can be explained by left-lateral faulting that is thought to accompany larger-scale clockwise block rotations within zones of distributed deformation (Ron et al., 1986). A similar mechanism has been used to explain localized to regional-scale faulting in the intracontinental Aegean region (McKenzie and Jackson, 1986). A similar mechanism was also used to explain the faulting within the Arakapas transform (MacLeod and Murton, l993; 1995), although it should be pointed out that published kinematic fault data remain sparse. It should also be noted that continuum-type models (e.g., Scott et al., 2012) may be applicable to cases, possibly including the Arakapas Fault Zone, where blocks are relatively small and where rotational stress increases towards a major bounding surface (e.g., Lamb, l987).

In summary, the presently available structural and palaeomagnetic data are consistent with right-lateral slip at a left-offset spreading axis (Fig. 21b).

ROLE OF EXTENSION WITHIN THE TRANSFORM

Several factors suggest that an extensional setting existed in the vicinity of and within the Arakapas transform during the time of clockwise dyke rotation: 1. Preferential intrusion of plagiogranite at an early stage, compared to the minor later stage intrusion along the northern margin of the Troodos Massif; 2. Intrusive relations of the late-stage brown dykes (e.g., sinuosity, bifurcation and space infill); 3. Relative abundance of boninite-type magmatism, possibly reflecting the ease of egress into the transform zone; 4. The presence of numerous normal faults throughout the road section studied.

A key feature of the left-slipping, right-offset transform model (Fig. 21c) is the inferred existence of major low-angle extensional faults (extensional detachments). A major low-angle extensional detachment fault, the Akapnou Forest Detachment has indeed been mapped within the eastern outcrop of the Arakapas Fault Zone (MacLeod, 1990). This fault zone separates upper crustal units made up of sheeted dykes, plus subordinate extrusive rocks or gabbro from underlying ultramafic rocks, which are mostly serpentinised harzburgite.

Rather than occurring specifically at the spreading ridge-transform intersection, MacLeod (1990) inferred that low-angle faulting continued over a long period, both prior to and during the accumulation of the Late Cretaceous (Santonian-Campanian) deep-sea sedimentary cover; i.e. for > 10 Ma after spreading of the Troodos ophiolite (around ~ 90 Ma; Turonian), as dated by Mukasa and Ludden (l987). It has also been suggested that the related extension relates to the relatively late-stage anticlockwise rotation of the Troodos ophiolite (see Murton, l990), as dated by Clube and Robertson (l986) and Morris et al. (1990).

Palaeomagnetic studies of sheeted dykes to the north of the Arakapas Fault Zone, to the west of the area studied; i.e. in the Mandria area (MacLeod et al., 1990) and also to the east of the area studied, in the SE Troodos (Allerton, 1988) show that relatively early dykes were rotated to a greater amount than crosscutting, later dykes. According to Gass et al. (1994), the main clockwise rotations pre-dated the late-stage boninite-type magmatism. A fault-disrupted unconformity is mapped within the transform zone, between rotated non-boninitic magmatic rocks and less rotated or non-rotated overlying boninitic rocks (lavas and dykes), utilising structural and palaeomagnetic data. In the section studied here, the relatively late-stage brown dykes show increasing vertical-axis rotations towards the Arakapas transform (Fig. 15). The dyke rotation is inferred to have taken place at the ridge-transform intersection (non-boninitic), followed by boninitic magmatism within the transform fault zone in an extensional or transtensional setting.

Cann et al. (2001) further infer that major extension took place at a very early stage at the spreading axis-transform intersection. They compare the extension to that observed along modern transform faults, such as the Atlantis Transform (Cann et al., 1997; Blackman et al., 1998). Cann et al. (2001) cite the occurrence of serpentinite clasts within sediments of the inferred upper plate of their detachment as evidence that the lower plate was exposed and eroded on the ocean floor. However, such ultramafic material has so far been reported only very locally from along the southern margin of the Limassol Forest Block (near Akrounda) (Gass et al., 1994). Rather than being serpentinite-rich the clastic sediments within the transform zone are dominated by basalt and diabase (Simonian and Gass, 1978; Gass et al., 1994). Fine-grained ferruginous sediments that are interbedded with lavas lack geochemical evidence of an ultramafic provenance (e.g., high Cr; high Ni) (see Robertson, 1978). On the other hand new evidence that is presented below shows that ultramafic rocks were indeed emplaced within the transform zone if it is accepted that this included serpentinite lineaments which are exposed within the Moni Mélange further south.

Cann et al. (2001) inferred the presence of three extensional detachments based on a reinterpretation of the geological map of the eastern outcrop of the Arakapas Fault Zone, as published by Gass et al. (1991). The extensional faults were inferred to cut downwards through the ophiolitic pseudostratigraphy towards the west, implying down-to the-west extension. This would be compatible with extensional exhumation taking place at the western inside corner strip of a ridge-transform intersection (see Fig. 21c). Whether any original down-to-the west extensional fault blocks would have survived the clockwise rotations documented by Morris et al. (1990) is debatable. The interpretative sections of Cann et al. (2001) appear to differ significantly from the original mapping published by Gass et al. (1991), for example in the structural order and thus kinematic significance of some units (e.g., west of Pevkos). The detachment surface was described by MacLeod (1990) as a single regionally extensive horizon that dips southwards at angles of several degrees rather than as three separate dipping detachments, as inferred by Cann et al. (2001). It would be useful to remap the area in question and obtain additional fault kinematic data to help distinguish between the different interpretations.

The interpretations of right (westward)-slipping exhumation along a right-offset ridge-transform intersection (Cann et al., 2001) might theoretically be reconciled with clockwise rotations resulting from ball-bearing-type rotations but only if a change in slip direction from left lateral to right lateral had taken place. Strike-slip reversal has been suggested in view of the reported evidence of opposing fault-slip directions within the Arakapas Fault Zone (Grand et al., 1993). However, most of the presently available structural evidence (MacLeod and Murton, 1993; 1995, and this study) is consistent with right-lateral slip within the transform fault zone as a whole, as in Fig. 21b.

Localised angular discordances and soft-sediment deformation of the Santonian-Campanian-aged metalliferous umbers and radiolarites (Perapedhi Formation) within the Arakapas Fault Zone, are locally observable above sea-floor sedimentary basaltic breccias (e.g., at Drapia and Layia) (Robertson, 1975; MacLeod, 1990). Such features could reflect reactivation of the Arakapas Fault Zone in a fracture zone setting outwith the offset spreading axes. One option is that the sediment instability was a consequence of the Campanian-Early Eocene anticlockwise rotation of the Troodos microplate (Morris et al., 1990; Morris, 1996).

TRANSFORM-RELATED OCEAN-FLOOR EXHUMATION

Despite the apparent difficulties with the outside corner detachment model (Cann et al., 2001; Fig. 21c), when the adjacent region to the south is considered there is additional evidence of ocean floor exposure of transform related crust. The Arakapas Fault Zone is widely considered to extend over several tens of kilometres from the bounding Arakapas Fault in the north to near, or beyond, the edge of the sedimentary cover in the south (Clube and Robertson, 1986; Gass et al., 1994; Cann et al., 2001). The inferred, opposing oceanic plate ('anti-Troodos plate') has been largely removed and tectonically replaced by the Late Cretaceous Moni Mélange (Robertson, 1977c; Clube and Robertson, 1986). The Moni Mélange includes ~ east to west-trending fault-bounded strips of dominantly serpentinised harzburgite (Robertson, 1977c; Fig. 1). These rocks have been correlated with the Arakapas Fault Zone or its lateral extension, as recognised in western Cyprus (Robertson, 1977b; Clube and Robertson, 1986; Morris et al., 1998).

To investigate the role of the serpentinised harzburgites within the Moni Mélange the best-exposed area (north of the junction between the roads to Pyrgos and Parekklisia) was mapped in detail, as shown in Fig. 22. The outcrop is dominated by mantle harzburgite, and is cut by minor gabbroic, to locally pegmatitic dyklets, similar to those exposed in places within the Arakapas Fault Zone (e.g., N of Akrounda). The serpentinite and the dyklets are cut by a network of dilational veins (mostly centimetres wide) which are infilled with fine-grained pink calcilutite. The network of veins affects the entire outcrop, reflecting an original thickness of tens of metres of oceanic crust. This sediment is interpreted as pelagic carbonate, although thin sections did not reveal any preserved microfossils, possibly owing to difficulties of preservation (e.g., diagenetic dissolution). Similar fine-grained carbonate sediment has been found infilling fissures, for example off Newfoundland, in the lower plate of an oceanic extensional detachment along the rifted North Atlantic margin (Robertson, 2007).

The fissured plutonic rocks (Fig. 22) are covered, depositionally, by debris-flow deposits, up to 10 m thick.

The clasts in these coarse deposits are dominated by serpentinised ultramafic rock, plus gabbro and rare chromitite, together with chaotically deformed inclusions of metalliferous sediments (umber). Individual serpentinite and gabbro clasts range from sub-angular to sub-rounded and are up to tens of centimetres in size. Some of the clasts include sediment-infilled fissures. The metalliferous sediment (umber) is smeared out within the matrix-supported conglomerates showing that it was redeposited while still poorly consolidated. On the other hand, basaltic clasts are absent from the debris flows, which is surprising because elsewhere the metalliferous umbers of the Troodos ophiolite are underlain by extrusive rocks (e.g., Robertson, 1975). Redeposition of umber would be expected to have entrained lava debris. After formation, the debris-flows were sheared and internally faulted. The ophiolitic body as a whole is in tectonic contact with mudrocks making up the matrix of the Moni Mélange (Fig. 22), which is dated as late Campanian-early Maastrichtian (Lord et al., 2000).

It is inferred here that the serpentinite and its associated lithologies (Fig. 22) formed within the general setting of the oceanic transform fault zone. The original location of formation of the fissured and sedimented-over mantle could have been near its present position to the south of the Arakapas Fault Zone, which would imply that the basaltic lavas of the 'anti-Troodos' plate (to the north of the Moni Mélange) belong to the transform fault zone as a whole. Alternatively, the exhumed mantle could have originated along a lateral extension of the transform, presumably to the east, assuming model b in Fig. 21 (in present co-ordinates). In either case, the strip of depleted mantle was tectonically incorporated into the Moni Mélange.

The field relations, therefore, show that ultramafic rocks of inferred transform affinities were exhumed to the ocean floor and fissured in an extensional (or transtensional) setting. This was followed by pelagic carbonate infill of the fissure system.

The area of exposed ultramafic crust is likely to have been restricted to the transform fault zone. However it became exposed, the depleted mantle rocks are likely to have been directly covered by metalliferous sediments, which elsewhere cover lavas. This, in turn, implies that depleted mantle was already exposed on the seafloor sufficiently near to the spreading axis to be directly covered by hydrothermal metalliferous sediments. The exhumed ultramafic rocks, together with their inferred metalliferous sediment cover, were then locally reworked on a rugged seafloor as serpentinite-dominated debris flows and sands. The exhumed serpentinite and its conglomeratic cover were then strongly sheared, possibly related to tectonic incorporation into the Moni Mélange during late Campanian-early Maastrichtian time.

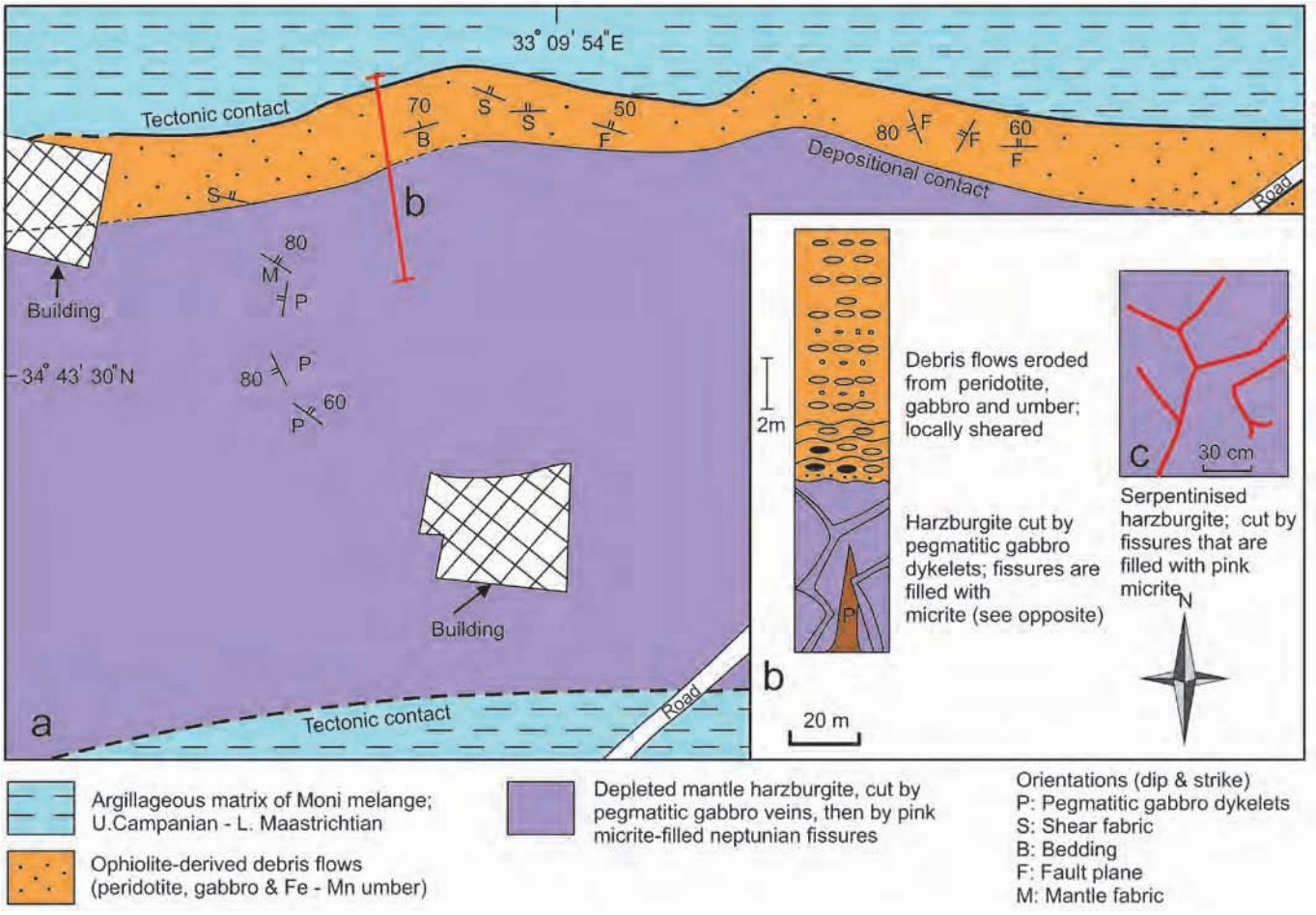

Fig. 22 - Geological map of part of an elongate ophiolitic inclusion within the Late Cretaceous Moni Mélange to the south of the Arakapas Transform Fault Zone (see Fig. 1). The field relations document exhumation, seafloor exposure and erosion of mantle harzburgite within an inferred oceanic transform setting. See Fig. 1 for location and the text for explanation.

The available evidence, therefore, suggests that a broad transform fault zone lay to the south of the Troodos plate (in present co-ordinates) and that this was associated with relatively early stage (i.e. pre-late Campanian) ocean floor extension or transtension, leading to localised crustal exhumation, exposure and erosion of mantle rocks on the seafloor. The overall setting is compatible with a left-offset spreading axis, as in model B in Fig. 21, but with a greater amount of extension than previously envisioned.

CONCLUSIONS

Related to the north-Troodos sheeted complex:

1. Sheeted dyke orientation changes from eastward dipping to westward dipping in the vicinity of a major shear zone, correlated with the western margin of the Solea Graben.
2. Hydrothermally generated epidosites with disseminated sulphide formed relatively early in the relative chronology of intrusion.
3. Minor plagiogranite dykes intruded after much intrusion and extensional faulting, but still near the spreading axis. Dyke intrusion was followed by pronounced amagmatic extension, for example forming the boundary between the Stavros and Solea Grabens.
4. There is a general magmatic trend towards highly depleted boninite-type magmatism which is assumed to have fed the Upper Pillow Lavas.

Related to the south-Troodos margin and the adjacent Arakapas Transform Fault Zone:

5. Plagiograntites intruded early as relatively large bodies (> 10s m), followed by localised intrusion of gabbro and then by predominant grey sheeted dykes; these were followed by isolated brown dykes and rare boninitic dykes (in the south).
6. Despite, their different appearances in outcrop, both the grey and the brown dykes are made up of compositionally similar tholeiitic basalts.
7. The measured clockwise swing in dyke trend towards E-W indicated that rotation (about a vertical axis) took place after dyke intrusion in the section studied. In addition, early-stage grey dykes and late-stage brown dykes are indicative of complex rotations (locally in opposing directions) near the Arakapas transform.
8. Faults with observable kinematic indicators are commonly left-lateral and tend to be orientated sub-parallel to the Arakapas transform to the south. The left-lateral faults are compatible with the clockwise rotation of large-scale tectonically bounded blocks.
9. Field evidence from an inferred extension of the Arakapas transform zone, now within the Late Cretaceous Moni Mélange, is indicative of the exhumation, exposure and submarine erosion of oceanic mantle harzburgite (and minor gabboic rocks).
10. The Troodos sheeted complex formed at an unstable spreading axis above a subduction zone. The spreading was accompanied or followed by regionally distributed amagmatic extension. The spreading crust was bounded by a right-slipping transform fault zone, which includes evidence of extensional exhumation of mantle rocks.

ACKNOWLEDGEMENTS

Lee Masson and Alastair Robertson thank Dr Costas Xenophontos for introducing them to the north-Troodos (Pyrgos) road transect. We are grateful to Dr. Nick Odling for assistance with the XRF analyses. Thanks are due to Profs. Chris MacLeod and Tony Morris for informative discussions. Mrs. Yvonne Cooper and Dr. Gillian McCay kindly assisted with the revision of diagrams. The manuscript benfitted from comments by two anonymous referrees.

REFERENCES

Abelson M., Baer G. and Agnon A., 2002. Fossil ridge-transform intersection in the Troodos ophiolite: New perspectives from rock magnetism in the gabbro suite and fracture mechanics analysis. Geochem. Geophys. Geosys, 3 (8): 1-17.

Allerton S., l988. Palaeomagnetism and structural studies of the Troodos ophiolite, Cyprus. In: C. Kissel and C. Laj, (Eds.), Palaeomagnetic rotations and continental deformation. NATO ARI Series, C, 254, p. 393-410.

Allerton S. and Vine F.J., 1987. Spreading structure of the Troodos ophiolite, Cyprus: Some paleomagnetic constraints. Geology, 15: 593-597.

Allerton S. and Vine F.J., 1990. Palaeomagnetic and structural studies of the southeastern part of the Troodos complex. In: J. Malpas, E.M. Moores, A. Panayiotou and C. Xenophontos (Eds.), Ophiolites: oceanic crustal analogues. Cyprus Geol. Surv. Dept., p. 99-111.

Allerton S. and Vine F.J., 1991. Spreading evolution of the Troodos ophiolite, Cyprus. Geology, 19 (6): 637-640.

Baragar W.R.A., Lambert N., Baglow N. and Gibson I.L., 1989. Sheeted dykes from CY-4 and surface sections: Troodos ophiolite. In: I.L. Gibson, J. Malpas, P.T. Robinson and C. Xenophontos (Eds.), Cyprus Crustal Study Project: Initial Report, Hole CY-4, Geol. Surv. Can., Paper 88-9: 69-106.

Baragar W.R.A., Lambert N., Baglow N. and Gibson I.L., 1990. The sheeted dyke zone in the Troodos ophiolite, In: J. Malpas, P.T. Robinson and C. Xenophontos (Eds.), Ophiolites and oceanic crustal analogues: Nicosia, Cyprus, Geol. Surv. Dept., Ministry of Agriculture and Natural Resources, p. 53-64.

Bednarz U. and Schmincke H.-U., 1989. Mass transfer during subseafloor alteration of the upper Troodos crust (Cyprus). Contrib. Mineral. Petrol., 102: 93-101.

Bettison-Varga L.,Varga R.J. and Schiffman P., l992. Relation between ore-forming hydrothermal systems and extensional deformation in the Solea graben spreading center, Troodos ophiolite, Cyprus. Geology, 20: 987-990.

Blackman D.K., Cann J.R., Janssen R., and Smith D.K., l998. Origin of extensional core complexes: Evidence from the Mid-Atlantic Ridge at Atlantis Fracture Zone, J. Geophys. Res. (Solid Earth), 103: 21,315-21,333.

Bonhommet N., Roperch P. and Calza F., 1988. Paleomagnetic arguments for block rotations along the Arakapas fault (Cyprus). Geology, 16: 422-425.

Borradaile G.J. and Gauthier D., 2006. Magnetic studies of magma-supply and sea-floor metamorphism: Troodos ophiolite dikes. Tectonophysics, 418: 75-92.

Cameron W., 1985. Petrology and origin of primitive lavas from the Troodos ophiolite, Cyprus. Contribs. Mineral. Petrol., 89: 239-255.

Cann J.R., Blackman D.K. Smith, E., McAllister, B., Janssen, S., Mello E., Avgerinos A.R. Pascoe and Escartin J., l997. Corrugated slip surfaces formed at ridge-transform intersections on the Mid-Atlantic Ridge. Nature, 385: 329-332.

Cann J.R. and Gillis K.M., 2004. Hydrothermal insights from the Troodos ophiolite, Cyprus, In: H. Elderfield and E. Davis (Eds.), The hydrology of the oceanic lithosphere. Cambridge Univ. Press, p. 274-310.

Cann J.R., Prichard H.M., Malpas J.G. and Xenophontos C., 2001. Oceanic inside corner detatchments of the Limassol Forest area, Troodos ophiolite, Cyprus. J. Geol. Soc. London, 158: 757-767.

Cannat M., Sauter D., Mendal V., Ruellan E., Okino K., Escartin J., Combin V. and Baala M., 2006. Modes of seafloor generation at a melt-poor ultraslow-spreading ridge. Geology, 34: 605-608.

Clube T., Creer K. and Robertson A. 1985. Palaeorotation of the Troodos microplate, Cyprus. Nature, 317: 522-525.

Clube T.M.M. and Robertson A.H.F., 1986. The paleorotation of the Troodos microplate, Cyprus, in the Late Mesozoic-Early Cenozoic plate tectonic framework of the eastern Mediterranean. Surv. Geophys., 8: 375-437.

Cooke A.J., 2013. Nature and implications of the sheeted dyke sequence within the northern margin of the Southern Troodos Transform Fault Zone, Cyprus. Unpubl. Univ. Edinburgh Masters Geol. Dissert.

Dietrich D. and Spencer S., 1993. Spreading-induced faulting and fracturing of oceanic crust: examples from the sheeted dyke complex of the Troodos ophiolite, Cyprus. In: H.M. Prichard, T. Alasbaster, N.B.W. Harris and C.R. Neary (Eds.), Magmatic processes and plate tectonics. Geol. Soc. London Spec. Publ., 76: 121-139.

Desmet A., Lapierre H., Rocci G., Gagny C., Parrot J.-F. and Delaloye M., 1978. Constitution and significance of the Troodos sheeted complex. Nature, 273: 527-530.

Fitton J.G. and Goddard M., 2004. Origin and evolution of magmas on the Ontong Java Platform. In: J.G. Fitton, J.J. Mahoney, P.J. Wallace and A.D. Saunders (Eds.), Origin and evolution of the Ontong Java Plateau. Geol. Soc. London Spec. Publ., 229: 151-178.

Fitton J.G., Saunders A.D., Larsen L.M., Hardarson B.S. and Norry M.J., 1998. Volcanic rocks from the southeast Greenland margin at 630N: composition, petrogenesis and mantle sources. Proceed. O.D.P. Sci. Results, 152: 331-350.

Gallo D.G., Fox P.J. and Macdonald K.C., 1986. A Sea Beam investigation of the Clipperton transform fault: The morphotectonic expression of a fast slipping transform boundary. J. Geophys. Res., 91: 3,455-3,467.

Gass I.G., 1968. Is the Troodos Massif of Cyprus a fragment of Mesozoic Ocean floor? Nature, 221: 926-930.

Gass I.G., MacLeod C.J., Murton B.J., Panayioutou A., Simonian K.O. and Xenophontos C., 1991. Geological map of the South Troodos Transform Fault Zone at 1:25000: Sheets 1 (west) and 2 (east). Geol. Surv. Dept. Nicosia, Cyprus.

Gass I.G., MacLeod C.J., Murton B.J., Panayiotou A., Simonian K.O. and Xenophontos C., 1994, Geology of the Southern Troodos transform fault zone, Cyprus. Cyprus Geol. Surv. Dept. Mem., 9, 214 pp.

Gee J., Varga R., Gallet Y. and Staudigel H., 1993. Reversed-polarity overprint in dikes from the Troodos ophiolite: Implications for the timing of alteration and extension. Geology, 21: 849-852.

Gillis K.M. and Robinson P.T., 1990. Patterns and processes of alteration in the lavas and dykes of the Troodos Ophiolite, Cyprus. J. Geophys. Res., 95: 523-548.

Grand T., Lapierre H., Mascle G.H., Ohnenstetter M. and Angelier J., 1993. Superimposed tectonics of the Cyprus ophiolitic massifs. Tectonics, 12: 93-101.

Granot R., Aleeson M., Ron H. and Agnon A., 2006. The oceanic crust in 3D: Paleomagnetic reconstruction in the Troodos ophiolite gabbro. Earth Planet. Sci. Lett., 251: 280-292.

Hurst S.D., Moores E.M. and Varga R.J., l994. Structural and geophysical expression of the Solea graben, Troodos Ophiolite, Cyprus. Tectonics, 13 (1): 139-156.

Karson J.A. and Lawrence R.M., l997a. Tectonic window into gabbroic rocks of the middle oceanic crust in the MARK area near sites 921-924, Proceed. O.D.P. Sci. Results, 153: 61-76.

Karson J.A. and Lawrence R.M., l997b. Tectonic setting of serpentinite exposures on the western median valley wall of the MARK area in the vicinity of site 920. Proceed. O.D.P. Sci. Results, 153: 5-21.

Kelley D.S., Robinson P.T. and Malpas J.G., 1992. Processes of brine generation and circulation in the oceanic crust: fluid inclusion evidence from the Troodos Ophiolite, Cyprus. J. Geophys. Res., 97: 9,307-9,322.

Kidd R.G.W. and Cann J.R., 1974. Chilling statistics indicate an ocean-floor spreading origin for the Troodos Complex, Cyprus. Earth Planet. Sci. Lett., 24: 151-155.

Kinnaird T.C. and Robertson A.H.F., 2013. Neogene tectonics and basin architecture of the southern margin of the Mesaoria Basin: implications for the southern margin of the Anatolian plate. In: A.H.F. Robertson, O. Parlak and Ü.C. Ünlügenç (Eds.), Geological development of the Anatolian continent and the northeasternmost Mediterranean region. Geol. Soc. London Spec. Publ., 372: 585-614.

Lamb S., 1987. A model for tectonic rotations about a vertical axis. Earth Planet. Sci. Lett., 84: 75-86.

Livermore R.A, Tomlinson J.S. and Wollett R.W, l991. Unusual sea-floor farbic near the Bullard fracture zone imaged by GLORIA sidescan sonar. Nature, 353: 258-161.

Lord A.R., Panayides A., Urquhart E. and Xenophontos C., 2000. A biostratigraphical framework for the Late Cretaceous - Recent circum-Troodos sedimentary sequence, Cyprus. In: I. Panayides, C. Xenophontos and J. Malpas (Eds.), Proceed. 3rd Internal Conference on the Geology of the Eastern Mediterranean. Cyprus Geol. Surv. Dept., p. 289-298.

Macdonald K., Castillo D.A., Miller S.P., Fox P.J., Kastens K.A. and Bonatti E., 1986. Deeptow studies of the Vema Fracture Zone: 1. Tectonics of a major slow slipping transform fault and its intersection with the Mid Atlantic Ridge. J. Geophys. Res. (Solid Earth) (1978-2012), 91: 3334-3354.

MacLeod C.J., 1990. Role of the Southern Troodos transform fault in the rotation of the Cyprus microplate: Evidence from the eastern Limassol Forest complex, In: J. Malpas, E.M. Moores, A. Panayiotou and C. Xenophontos (Eds.), Proceed. Symposium on Ophiolites and Oceanic Lithosphere, Troodos 87. Nicosia, Cyprus. Cyprus Geol. Surv. Dept., p. 75-85.

MacLeod C.J., Allerton S., Gass I.G. and Xenophonotos C., 1990. Structure of a fossil ridge-transform intersection in the Troodos ophiolite. Nature, 348: 717-720.

MacLeod C.J. and Murton B.J., 1993. Structure and tectonic evolution of the Southern Troodos Transform Fault Zone, Cyprus. In: H.M. Prichard, T. Alasbaster, N.B.W. Harris and C.R. Neary (Eds.), Geol. Soc. London Spec. Publ., 76: 141-176.

MacLeod C.J. and Murton B.J., 1995. On the sense of slip of the Southern Troodos transform fault zone, Cyprus. Geology, 23: 257-260.

Maguire P.K.H., Coogan L.A., Khan M.A., Eaton M. and Petides G., 2006. Geophysical constraints on the crustal architecture of the Troodos ophiolite: results from the IANGASS project. Geophys. J. Intern., 167 (3): 1385-1401.

McKenzie D.P. and Jackson J.A., l986. A block model of distributed deformation by faulting. J. Geol. Soc. London, 143: 349-353.

Malpas 1990. Crustal accretion processes in the Troodos ophiolite, Cyprus: evidence from field mapping and deep crustal drilling. In: J. Malpas, E.M. Moores, A., Panayiotou, A. and C. Xenophontos (Eds.), Ophiolites: Oceanic crustal analogues. Cyprus Geol. Surv. Depart., p. 65-74.

Masson L., 2012. Structure of the western Solea Graben, growth by listric faults in a fast spreading regime and injection of differentiated dyke suites constrained by rotated fault blocks: Troodos Sheeted Dyke complex, Cyprus. Unpubl. Univ. Edinburgh Masters Geol. Dissert.

Moores E.M., Varga R.J., Verosub K.L. and Ramsden T., l990. Regional structure of the Troodos dyke complex. In: J. Malpas, E.M. Moores, A. Panayiotou, and C. Xenophontos (Eds.), Ophiolites: Oceanic crustal analogues. Cyprus Geol. Surv. Dept., p. 27-35.

Moores E.M. and Vine F.J., 1971. The Troodos Massif, Cyprus and other ophiolites as oceanic crust: evolution and implications. Phil. Trans. R. Soc. London (Ser. A), Math. Phys. Sci., 268: 443-467.

Morris A., 1996. A review of palaeomagnetic research in the Troodos ophiolite, Cyprus. In: A. Morris and D.H. Tarling (Eds.), Palaeomagnetism and tectonics of the Mediterranean region. Geol. Soc. London Spec. Publ., 105: 311-324.

Morris A., Anderson M.W. and Robertson A.H.F., 1998. Multiple tectonic rotations and transform tectonism in an intraoceanic suture zone, S.W. Cyprus. Tectonophysics, 299: 229-253.

Morris A., Creer K.M. and Robertson A.H.F., 1990. Palaeomagnetic evidence for clockwise rotations related to dextral shear along the Southern Troodos Transform Fault, Cyprus. Earth Planet. Sci. Lett., 99: 250-262.

Mukasa S.B. and Ludden J.N., 1987, Uranium-lead isotopic ages of plagiogranites from the Troodos ophiolite, Cyprus, and their tectonic significance. Geology, 15: 825-828.

Mullen E.D., 1983. $MnO/TiO_2/P_2O_5$: a minor element discriminant for basaltic rocks of oceanic environments and its implications for petrogenesis. Earth Planet. Sci. Lett., 62: 53-62.

Murton B., 1986. Anomalous oceanic lithosphere formed in a leaky transform fault: evidence from the Western Limassol Forest Complex, Cyprus. J. Geol. Soc. London, 143: 845-854.

Murton B., 1989. Tectonic controls on boninite genesis. In: A.D. Saunders and M.J. Norry (Eds.), Magmatism in the ocean basins. Geol. Soc. London Spec. Publ., 42: 347-377.

Murton B.J., 1990. Was the Southern Troodos Transform Fault a victim of microplate rotation? In: J. Malpas, E.M. Moores, A. Panayiotou and C. Xenophontos (Eds.), Ophiolites: Oceanic crustal analogues. Cyprus Geol. Surv. Dept., p. 87-98.

Nicholson C., Seeber L., Williams P. and Sykes L.R., 1986a. Seismicity and fault kinematics through the eastern Transverse Ranges, California: block rotation, strike-slip faulting and low-angle thrusts. J. Geophys. Res., 91, B5: 4,891-4,908.

Nicholson C., Seeber L., Williams P. and Sykes L.R., 1986b. Seismic evidence for conjugate slip and block rotation within the San Andreas fault system, southern California. Tectonics, 5: 629-648.

Nuriel P., Katzir Y., Abelson M., Valley J.W., Matthews A., Spicuzza M.J. and Ayalon A., 2009. Fault-related oceanic serpentinization in the Troodos ophiolite, Cyprus: Implications for a fossil oceanic core complex. Earth Planet. Sci. Lett., 282: 34-46.

Pearce J.A., 1975. Basalt geochemistry used to investigate past tectonic environment on Cyprus. Tectonophysics, 25: 443-466.

Pearce J.A., l982. Trace element characteristics of lavas from destructive plate boundaries. J. Wiley & Sons, Chichester, p. 525-548.

Pearce J.A., 1996. A user's guide to basalt discrmination diagrams. In: D.A. Wyman (Ed.), Trace element geochemistry of volcanic rocks: Applications for massive sulphide exploration. Geol. Assoc. Can., Short Course Notes, 12: 79-113.

Pearce J.A. and Cann J.R., 1973. Tectonic setting of basic volcanic rocks determined using trace element analysis. Earth Planet. Sci. Lett., 19: 290-300.

Pearce J.A, Lippard S.J. and Roberts S., 1984. Charicteristics and tectonic significance of supra-subduction zone ophiolites. In: B.P. Kokelaar and M.F. Howells (Eds.), Marginal basin geology. Geol. Soc. London Spec. Publ., 76: 77-94.

Pearce J.A. and Robinson P., 2010. The Troodos ophiolitic complex probably formed in a subduction initiation, slab edge setting. Gondwana Res., 18: 60-81.

Phillips-Lander C.M. and Dilek Y., 2009. Structural architecture of the sheeted dike complex and extensional tectonics of the Jurassic Mirdita ophiolite, Albania. Lithos, 108: 192-206.

Richardson C., Cann J., Richards H. and Cowan J., 1987. Metal-depleted root zones of the Troodos ore-forming hydrothermal systems, Cyprus. Earth Planet. Sci. Lett., 84: 243-253.

Robertson A.H.F., 1975. Cyprus umbers: basalt-sediment relationships on a Mesozoic ocean ridge. J. Geol. Soc., London, 131: 511-531.

Robertson A.H.F., l977a. Tertiary uplift history of the Troodos massif, Cyprus. Geol. Soc. Am. Bull., 88: 1763-1772.

Robertson A.H.F. 1977b. The Kannaviou Formation, Cyprus: volcaniclastic sedimentation of a probable Late Cretaceous volcanic arc. J. Geol. Soc. London, 134: 269-292.

Robertson A.H.F., 1977c. The Moni Mélange, Cyprus: an olistostrome formed at a destructive plate margin. J. Geol. Soc. London, 133: 447-66.

Robertson A.H.F., 1978. Metallogenesis along a fossil oceanic fracture zone: Arakapas fault belt, Troodos Massif, Cyprus. Earth Planet. Sci. Lett., 41: 317-329.

Robertson A.H.F., 1990. Tectonic evolution of Cyprus. In: J. Malpas, E. Moores, A. Panayiotou and C. Xenophontos (Eds.), Ophiolites: oceanic crustal analogues. Proc. Symp. "Troodos 1987" Nicosia, Cyprus. Cyprus Geol. Surv. Dept., p. 235-252.

Robertson A.H.F., 2007. Geochemical evidence for the sedimentary and diagenetic development of the Mesozoic-early Cenozoic Newfoundland rifted margin, northwest Atlantic (Ocean Drilling Program Leg 210, Site 1276). In: B.E. Tucholke, J.-C. Sibuet and A. Klaus (Eds.), Proc. O.D.P. Sci. Results, 210: 1-63. doi:10.2973/odp.proc.sr.210.105.2007

Robertson A.H.F. and Xenophontos C., 1993. Development of concepts concerning the Troodos ophiolite and adjacent units in Cyprus. In: H.M. Prichard, T. Alasbaster, N.B.W. Harris and C.R. Neary (Eds.), Geol. Soc. London Spec. Publ., 76: 85-119.

Robinson P.T., Malpas J., Dilek Y. and Zhou M.-F., 2008. The significance of sheeted dike complexes in ophiolites. GSA Today, 18 (11): 4-10.

Ron H., Aydn A. and Nur., 1986. Strike-slip faulting and block rotations in the Lake Mead fault system. Geology, 14: 1,020-1,023.

Ron H. and Eyal Y., l985. Intra-plate deformation by block rotation and mesostructures along the Dead Sea Transform, Northern Israel, Tectonics, 4: 85-105.

Scottt C.P., Titus S.J. and Davis J.R., 2012. Using field data to constrain a numerical kinematic model for ridge-tranform deformation in the Troodos ophiolite, Cyprus. Lithosphere, 5 (1): 109-127.

Shervais J. W., 1982. Ti-V plots and the petrogenesis of modern and ophiolitic lavas. Earth Planet, Sci. Lett., 59: 101-118.

Smith D., 2013. Mantle spread across the sea floor. Nature Geosci., 6: 247-248.

Simmonian K.O. and Gass I.G. 1978. Arakapas fault belt, Cyrpus: A fossil transform fault. Geol. Soc. Am. Bull., 89: 1,220-1,230.

Sonder L.J. and Pockalny R.A., 1999. Anomalously rotated abyssal hills along active transforms: Distributed deformation of oceanic lithosphere. Geology, 2: 1003-1006.

Van Everdingen D.A. and Cawood P.A., l995. Dyke domains in the Mitsero graben, Troodos ophiolite, Cyprus: an off-axis model for graben formation at a spreading centre. J. Geol. Soc. London, 152: 923-932.

Varga R.J., Gee J.S., Bettison-Varga L., Anderson R.S. and Johnson C.L., l999. Early establishment of seafloor hydrothermal systems during structural extension: paleomagnetic evidence from the Troodos ophiolite, Cyprus. Earth Planet. Sci. Lett., 171: 221-235.

Varga R. and Moores E., 1985. Spreading structure of the Troodos Ophiolite, Cyprus. Geology, 13: 846-850.

Varga R.J. and Moores E.M., 1990. Intermittant magmatic spreading and tectonic extension in the Troodos Ophiolite: implications for exploration for black smoker-type ore deposits. In: J. Malpas, E.M Moores, A. Panayiotou and C. Xenophontos (Eds.), Ophiolites: oceanic crustal analogues. Cyprus Geol. Surv. Dept., p. 53-64.

Veit K., 1996. Petrological investigation of the sheeted dike zone of the Troodos ophiolite, Cyprus. Keck Symp., 9: 245-252.

Wilson R.A.M. and Ingham P.T., l959. The geology of the Xeros-Troodos Area with an account of the mineral resources. Cyprus. Mem. Geol. Surv. Dept., 1: 1-184.

Received, January 7, 2014
Accepted, May 12, 2014